CERN-PH-TH/2004-022
FNT/T 2004/02

Comparisons of the Monte Carlo programs HORACE and WINHAC for single-W-boson production at hadron colliders*

C.M. Carloni Calame[a,b], **S. Jadach**[c,d], **G. Montagna**[b,a], **O. Nicrosini**[a,b] *and* **W. Płaczek**[e,d]

[a] *Istituto Nazionale di Fisica Nucleare, Sezione di Pavia*
Via A. Bassi 6, I-27100 Pavia, Italy.
[b] *Dipartimento di Fisica Nucleare e Teorica, Università di Pavia,*
Via A. Bassi 6, I-27100 Pavia, Italy.
[c] *Institute of Nuclear Physics, Polish Academy of Sciences,*
ul. Radzikowskiego 152, 31-342 Cracow, Poland.
[d] *Department of Physics, CERN, Theory Division, CH-1211 Geneva 23, Switzerland.*
[e] *Institute of Physics, Jagellonian University,*
ul. Reymonta 4, 30-059 Cracow, Poland.

Abstract

We present the comparisons of two independent Monte Carlo event generators, HORACE and WINHAC, for single-W-boson production in hadronic collisions with multiphoton effects in leptonic W decays. These comparisons were performed first at the parton level with fixed quark-beams energy, and then at the hadron level for proton–proton collisions at the LHC. In general, a good agreement between the two programs has been found. Possible sources of differences in some of the presented results are discussed. We also present and discuss the effects of including non-zero quark masses for the main single-W-boson observables at the LHC.

To be submitted to Acta Physica Polonica B

* Work partly supported by the Polish Government grants KBN 2P03B00122 and KBN 5P03B09320, the EC FP5 Centre of Excellence "COPIRA" under the contract No. IST-2001-37259 and the EC FP5 contract HPRN-CT-2000-00149.

CERN-PH-TH/2004-022
Februrary 2004

1 Introduction

The Large Hadron Collider (LHC) currently under construction at CERN, apart from its large discovery potential in high-energy physics, will also offer an opportunity for precision measurements of some important electroweak parameters, see e.g. Ref. [1]. Some of these measurements will be able to surpass even the high precision achieved by electron–positron colliders, such as LEP, see e.g. Ref. [2]. A particularly important role among these is played by the measurement of the W-boson mass and width. It will be performed during the first phase of running the LHC – with low luminosity. This improved measurement of the basic W-boson parameters will narrow down the mass window for the Higgs boson searches in the second phase of the LHC run and, of course, it will provide a more stringent test of the Standard Model. The main source of W-bosons at the LHC will be the process of single-W-boson production. To avoid the huge QCD background the LHC experiments will look only at leptonic W-decay channels, excluding τ's, which decay mainly hadronically. Huge rates of single-W (and single-Z) events that will be produced at the LHC during its first phase of running can also be exploited for measurements of parton distribution functions (PDFs) in the proton and parton luminosities [3].

In order to achieve the above experimental goals high-precision theoretical predictions are needed for the process of single-W-boson production with leptonic W decays, provided in terms of a Monte Carlo (MC) event generator. One of the goals of the CERN Workshop on Monte Carlo Tools for the LHC, held in the summer of 2003 at CERN [4], particularly its Electroweak Working Group, was to collect such event generators and to perform their basic comparative tests. The aim of these tests was to check both the technical and physical precision of the respective programs and to provide guidelines for their further improvements. None of the currenlty existing MC event generators includes all the ingredients that are necessary for the real experimental data analysis of the single-W events. They can, generally, be split into two classes: the programs that deal with the QCD effects and those dedicated to a precision description of QED/EW corrections [2].

Here we consider two MC event generators: HORACE [5] and WINHAC [6], which in their current versions include higher-order QED corrections in leptonic W-boson decays. Control over the QED correction in W decays is of crucial importance for the precision determination of the W mass and width at hadron colliders, see e.g. [7]. WINHAC and HORACE are the first MC event generators to go beyond $\mathcal{O}(\alpha)$ in accounting for these corrections.

We performed numerical comparisons of the above programs in two steps. In the first step, we compared their predictions at the pure parton level, for fixed initial quark energies. The processes considered in this step do not correspond directly to the ones studied in real-life experiments; however, such tests are useful for technical reasons. The QED corrections in leptonic W-boson decays are actually included in the parton-level processes; testing them at this level thus allows a direct check of their implementation, without any influence of additional effects (PDFs, QCD, etc.). One should, however, keep in mind that any differences seen at this level have a rather technical meaning and cannot be simply translated into realistic proton–proton collisions.

In the second step, the two programs were cross-checked at the hadron level, i.e. for proton–proton collisions at the LHC energies, where the basic parton-level hard processes were convoluted with the PDFs of the two colliding protons. In these comparisons we considered four single-W quantities: the W-boson transverse mass, the charged lepton transverse momentum, the W-boson pseudorapidity[1] and the charged lepton pseudorapidity. The first two are sensitive to the W-boson mass and width, the other two to the PDFs and the parton luminosities. In addition, we compared two photon observables: the hardest-photon transverse momentum and its pseudorapidity.

The paper is organized as follows. In Section 2 we briefly describe the two programs. In Sections 3 and 4 we present and discuss the comparisons at the parton level and at the hadron level, respectively. Section 5 is devoted to quark-mass effects on the main W-boson observables. Finally, Section 6 contains a summary and outlook of this work.

2 Programs

2.1 HORACE

HORACE [5] is a Monte Carlo event generator for the Drell–Yan-like processes $p\overset{(-)}{p} \to W \to l\nu_l$ and $p\overset{(-)}{p} \to \gamma, Z \to l^+l^-$, with $l = e, \mu$. In HORACE the corrections due to (real plus virtual) multiphoton radiation are computed using the well-known QED structure-function approach. The corrections are calculated by solving numerically the DGLAP evolution equation for the QED structure function by means of the parton shower algorithm described in detail in Refs. [8, 9].

Only the corrections relative to the subprocesses $W \to l\nu_l$ and $Z \to l^+l^-$ are at present included in HORACE, because it is known that quark-mass singularities, originating from initial-state photon radiation, can be reabsorbed into a redefinition of the PDFs, in analogy to gluon emission in QCD. HORACE can calculate photonic corrections to all orders and at $\mathcal{O}(\alpha)$, to disentangle the effect of higher-order contributions and to compare it with that of the available $\mathcal{O}(\alpha)$ programs. Technically speaking, the energy of the emitted photons is extracted from the Altarelli–Parisi $e \to e + \gamma$ splitting function, while the generation of the photons' angles is performed according to the factorized part of the radiation matrix element, which for the $W \to l\nu\gamma$ decay reads as [10] $(p/p\cdot k - Q/Q\cdot k)^2$, where p is the four-momentum of the final-state lepton l, k is the photon four-momentum, and Q is the four-momentum (virtuality) of the W boson.

Complete $\mathcal{O}(\alpha)$ electroweak corrections are not included in the present version of the generator, but work is in progress in order to make them available in a future release. To provide predictions at the hadron level, the parton-level subprocesses for W and Z production in quark–antiquark annihilation are convoluted with collinear PDFs from the PDFLIB package [11].

[1]The W-boson pseudorapidity is not measured in the real experiment since neutrino detection is lacking, however it can be useful for some generator-level studies.

2.2 WINHAC

WINHAC [6] is a Monte Carlo event generator for single-W-boson production in hadronic collisions (proton–proton and proton–antiproton) with leptonic W decays. Its main feature is the Yennie–Frautschi–Suura (YFS) $\mathcal{O}(\alpha)$ QED exponentiation in leptonic W-boson decays, described in detail in Ref. [12]. WINHAC generates multiphoton radiation in W decays, which is exact: (1) to all orders in the infrared (IR) limit and (2) up to $\mathcal{O}(\alpha)$ for non-IR contributions. The non-IR photonic contributions beyond $\mathcal{O}(\alpha)$ are included in an approximate way: some parts of leading-log as well as subleading terms are taken into account through the YFS exponentiation. The recent version of the program includes also the $\mathcal{O}(\alpha)$ electroweak (EW) corrections to the leptonic W decays [13], implemented within the YFS exponentiation scheme. The implementation of the full $\mathcal{O}(\alpha)$ EW corrections to the charged-current Drell–Yan process is under way.

The parton-level hard process of single-W production in quark–antiquark collisions is convoluted with the standard proton PDFs from the PDFLIB package [11] – to give a hadron–level process appropriate for proton–proton or proton–antiproton collisions. The Bjorken x's and Q^2 of the quark–antiquark pair are generated with the help of the self-adaptive MC sampler Foam [14]. QCD effects are included in the current version only trough scaling-violation of collinear PDFs (no quark p_T, no parton showers, no hadronization).

3 Parton-level comparisons

For the parton-level comparisons we considered the following processes:

$$d + \bar{u} \longrightarrow W^- \longrightarrow l^- + \bar{\nu}_l, \quad l = e,\, \mu, \tag{1}$$

with the $+z$ axis pointing in the incoming d-quark direction. Our MC calculations were done in the G_μ scheme and the fixed-width scheme, for the following input parameters:

$$\begin{aligned}
&m_d = 3 \times 10^{-3}\,\text{GeV}, \quad m_u = 6 \times 10^{-3}, \quad V_{ud} = 1, \quad m_{\nu_l} = 0,\\
&m_e = 0.511 \times 10^{-3}\,\text{GeV}, \quad m_\mu = 0.10565836\,\text{GeV}, \quad m_\tau = 1.77703\,\text{GeV},\\
&M_W = 80.423\,\text{GeV}, \quad M_Z = 91.1882\,\text{GeV}\\
&s_W^2 = 1 - \frac{M_W^2}{M_Z^2}, \quad \Gamma_W = \frac{3 G_\mu M_W^3}{2\sqrt{2}\pi}\left(1 + \frac{2\alpha_s}{3\pi}\right),\\
&\alpha^{-1} = 137.03599976, \quad G_\mu = 1.16639 \times 10^{-5}\,\text{GeV}^{-2}, \quad \alpha_s = 0.1185,\\
&E_{\text{CM}} = \sqrt{s} = M_W.
\end{aligned} \tag{2}$$

The results have been obtained for two kinds of event selection:

- **BARE** – where the corresponding observables were obtained from bare-lepton four-momenta and no cuts were applied.

- **CALO** – where the photon four-momenta were combined with the charged-lepton four-momenta if the opening angle between their directions $\angle(\vec{q}_l, \vec{k}) \leq 5^\circ$; such photons were discarded; no extra cuts were applied.

We considered only QED-like corrections to leptonic W-boson decays. Our computations were done at three levels: (1) Born, (2) $\mathcal{O}(\alpha)$ (as implemented in the respective programs), and (3) with higher-order corrections (the so-called "Best" predictions).

Program	σ^{tot} [nb]		
	Born	$\mathcal{O}(\alpha)$	Best
Electrons			
HORACE	8.88722 (00)	8.88721 (00)	8.88721 (0)
WINHAC	8.88715 (20)	8.88552 (12)	8.88401 (5)
$\delta = (\mathrm{W} - \mathrm{H})/\mathrm{W}$	$-0.8\,(2.3) \times 10^{-5}$	$-1.9\,(0.1) \times 10^{-4}$	$-3.60\,(0.06) \times 10^{-4}$
Muons			
HORACE	8.88722 (00)	8.88632 (1)	8.88632 (1)
WINHAC	8.88720 (13)	8.88533 (6)	8.88440 (5)
$\delta = (\mathrm{W} - \mathrm{H})/\mathrm{W}$	$-0.2\,(1.4) \times 10^{-5}$	$-1.11\,(0.07) \times 10^{-4}$	$-2.16\,(0.06) \times 10^{-4}$

Table 1: The parton-level results for the Born, the $\mathcal{O}(\alpha)$ and the "Best"-level total cross section in nanobarns [nb] from HORACE and WINHAC. The numbers in parentheses are statistical errors for the last digits.

In Table 1 we present the results for the total cross section from HORACE and WINHAC. As can be seen, the agreement between the two programs for the total integrated cross section without any cut is excellent, the relative differences being at the level of 10^{-4} both at the Born level and in the presence of QED corrections. The remaining differences of $\sim 2 \times 10^{-4}$ for the $\mathcal{O}(\alpha)$ and "Best" predictions can be explained by the different treatment of QED corrections in the structure-functions (SF) approach and the YFS exclusive exponentiation. In the SF calculations the net effect of the QED correction for the total cross section is zero (except for some small lepton-mass effects in the phase-space integration). In the YFS exponentiation, on the other hand, the QED corrections to the total cross section are non-zero due to subleading terms, which are at the level of $\sim 2 \times 10^{-4}$, as was shown in Ref. [12].

In the following we present the comparisons of various distributions. As a first step, we compared the Born-level distributions of lepton energy and polar angle for both the electron and muon channels, obtaining a very good agreement (within statistical errors corresponding to the same event samples, as presented in Table 1). The lepton energy and lepton angle distributions for $\mathcal{O}(\alpha)$ and "Best" predictions of the two programs, and when considering the BARE and CALO event selections, are shown in Figs. 1–4. For such distributions, the agreement between the two programs can be considered generally good. Actually, the differences are at the level of 1% in those regions of the differential distributions, yielding the dominant contribution to the integrated cross section, while they can reach the 10% (or more) level only in the kinematical regions that are dynamically and/or

kinematically suppressed. In Figs. 5–10 we present distributions of photonic observables: the hardest photon energy, the total photon energy (i.e. the sum of all radiative-photon energies), and the hardest photon polar angle. As for the leptonic distributions, the agreement is quite satisfactory since, whenever "large" differences are present, they occur in those regions that give only a small contribution to the integrated cross section. In particular, it can be seen from Figs. 5–8 that the agreeement is considerably better for the CALO event selection than for the BARE one, as expected as a consequence of the (partial) cancellation of leading-logarithmic corrections in the more inclusive CALO case.

As can be seen in Figs. 1–8, the differences between HORACE and WINHAC for their "Best" predictions are almost the same as the ones at $\mathcal{O}(\alpha)$. This indicates that the main effect comes from different treatment of the $\mathcal{O}(\alpha)$ subleading terms in the two programs. The differences become large in the regions of phase space where these subleading terms start to dominate. In these regions, however, the cross section is very small.

4 Hadron-level comparisons

For the hadron-level comparisons we considered the following processes:

$$\begin{aligned} pp &\longrightarrow W^- + X \longrightarrow l^- + \bar{\nu}_l + X, \\ pp &\longrightarrow W^+ + X \longrightarrow l^+ + \nu_l + X, \end{aligned} \tag{3}$$

where $l = e,\ \mu$. In this case, the parton-level processes of W production and decay were convoluted with the standard PDFs. For our tests we used the MRS(G) parametrization as provided by the PDFLIB package [11] (`Ntype = 1, Ngroup = 3, Nset = 41`). As in the parton-level case, our MC calculations were done in the G_μ scheme and the fixed-width scheme, for the following input parameters:

$$\begin{aligned} & m_e = 0.511 \times 10^{-3}\,\text{GeV}, \quad m_\mu = 0.10565836\,\text{GeV}, \quad m_{\nu_e} = m_{\nu_\mu} = 0 \\ & m_u = m_d = m_s = m_c = m_b = 0, \quad m_t = 174.3\,\text{GeV}, \quad m_H = 150\,\text{GeV}, \\ & V_{ud} = 0.97483, \quad V_{us} = 0.22290, \quad V_{ub} = 0.00360, \\ & V_{cd} = -0.22286, \quad V_{cs} = 0.97398, \quad V_{cb} = 0.04120, \\ & V_{td} = 0.00568, \quad V_{ts} = -0.04097, \quad V_{tb} = 0.99914, \\ & M_W = 80.423\,\text{GeV}, \quad M_Z = 91.1882\,\text{GeV} \\ & s_W^2 = 1 - \frac{M_W^2}{M_Z^2}, \quad \Gamma_W = \frac{3 G_\mu M_W^3}{2\sqrt{2}\pi}\left(1 + \frac{2\alpha_s}{3\pi}\right), \\ & \alpha^{-1} = 137.03599976, \quad G_\mu = 1.16639 \times 10^{-5}\,\text{GeV}^{-2}, \quad \alpha_s = 0.1185, \\ & E_{\text{CM}} = \sqrt{s} = 14\,\text{GeV}. \end{aligned} \tag{4}$$

We used the following event selection criteria:

- the charged lepton transverse momentum: $p_T^l > 25\,\text{GeV}$;
- the charged lepton pseudorapidity: $|\eta_l| < 2.4$;

- the missing transverse energy: $E_T^{\text{miss}} > 25\,\text{GeV}$ (we used $E_T^{\text{miss}} = p_T^{\nu}$);
- the size of an electron cluster (for electron–photon recombination): $\Delta\eta_e \times \Delta\phi_e = 0.075 \times 0.175\,\text{rad}$, where η_e and ϕ_e are the electron pseudorapidity and azimuthal angle;
- no photon recombination with muons.

For our main tests we chose four basic single-W observables:

1. W-boson transverse mass: m_T^W;
2. charged lepton transverse momentum: p_T^l;
3. W-boson rapididy: y_W;
4. charged lepton pseudorapidity: η_l.

The first two are important for the W mass and width measurement, the other two for the PDFs and parton-luminosity measurements.

As additional tests, we performed the comparisons of photonic distributions:

1. hardest photon transverse momentum: p_T^{γ};
2. hardest photon pseudorapidity: η_{γ},

for which we used additional cuts:

- photon transverse momentum: $p_T^{\gamma} > 25\,\text{GeV}$;
- photon pseudorapidity: $|\eta_{\gamma}| < 2.4$.

In Tables 2 and 3 we present the results for the total cross section from HORACE and WINHAC without cuts and with cuts (as described above), respectively. Except for the muon channels in the presence of the cuts, where the differences between the two programs are at the level of $\sim 10^{-3}$, the agreement between the two programs is consistent with the one at the parton level. The differences in the muon channels can be explained by the muon mass effects enhanced by the cuts. In WINHAC the non-zero muon masses are taken into account, while in HORACE the muon masses are neglected. It can also be noticed that the differences observed at the level of $\mathcal{O}(\alpha)$ cross sections still remain in the presence of higher-order corrections (the "Best" predictions). This clearly indicates a difference in the treatment of $\mathcal{O}(\alpha)$ subleading corrections, which is expected on the grounds of the different ingredients and formulation of the two generators, and an almost complete agreement for the size of higher-order contributions.

The comparisons of the distributions are shown in Figs. 11–22. The results for both the W^+ and W^- decays are shown. For the transverse mass and lepton transverse momentum distributions, as well as for the W rapidity and lepton pseudorapidity distributions, the differences are confined within 0.2%, indicating a very good agreement between the two

Program	$\sigma^{\rm tot}$ [nb]: WITHOUT CUTS		
	Born	$\mathcal{O}(\alpha)$	Best
$W^- \longrightarrow e^-\bar{\nu}_e$			
HORACE	7.73310 (39)	7.73314 (41)	7.73249 (43)
WINHAC	7.73315 (11)	7.73171 (07)	7.73039 (03)
$\delta = (\mathrm{W}-\mathrm{H})/\mathrm{W}$	$0.6\,(5.2)\times 10^{-5}$	$-1.8\,(0.5)\times 10^{-4}$	$-2.7\,(0.5)\times 10^{-4}$
$W^- \longrightarrow \mu^-\bar{\nu}_\mu$			
HORACE	7.73317 (39)	7.73322 (39)	7.73285 (41)
WINHAC	7.73317 (07)	7.73162 (04)	7.73075 (03)
$\delta = (\mathrm{W}-\mathrm{H})/\mathrm{W}$	$0.0\,(5.1)\times 10^{-5}$	$-2.1\,(0.5)\times 10^{-4}$	$-2.7\,(0.5)\times 10^{-3}$
$W^+ \longrightarrow e^+\nu_e$			
HORACE	10.93760 (56)	10.93804 (59)	10.93679 (61)
WINHAC	10.93684 (17)	10.93535 (12)	10.93322 (04)
$\delta = (\mathrm{W}-\mathrm{H})/\mathrm{W}$	$-6.9\,(5.4)\times 10^{-5}$	$-2.5\,(0.6)\times 10^{-4}$	$-3.3\,(0.6)\times 10^{-4}$
$W^+ \longrightarrow \mu^+\nu_\mu$			
HORACE	10.93757 (56)	10.93856 (57)	10.93683 (57)
WINHAC	10.93714 (11)	10.93507 (06)	10.93381 (04)
$\delta = (\mathrm{W}-\mathrm{H})/\mathrm{W}$	$-3.9\,(5.2)\times 10^{-5}$	$-3.2\,(0.5)\times 10^{-4}$	$-2.8\,(0.5)\times 10^{-4}$

Table 2: The hadron-level results for the Born, the $\mathcal{O}(\alpha)$ and the "Best"-level total cross section (in nb) from HORACE and WINHAC without cuts. The numbers in parentheses are statistical errors for the last digits.

programs for the observables relevant to the measurement of the W mass and width and for the parton-luminosity determination. For the electron channels the agreement is generally within the statistical errors, while for the muon channels there are systematic differences at the level 0.1–0.2%. They can be explained by the neglect of muon masses in HORACE, as in the case of the total cross section. For the photonic distributions, the differences can reach some per-cent level, which can again be ascribed to the different treatment of $\mathcal{O}(\alpha)$ subleading terms.

In Figs. 23–28 we show the size of the $\mathcal{O}(\alpha)$ and higher-order QED corrections for the above distributions. As can be seen, the predictions of $\mathcal{O}(\alpha)$ and higher-order QED corrections from the two programs are in good agreement, in both shape and size. It can in particular be observed that the contribution of QED corrections is almost flat for the W-boson rapidity and lepton pseudorapidity, as well as for the exclusive photon observables, whereas it is a varying function for the W-boson transverse mass spectrum and the lepton transverse momentum distribution. In the two latter cases, the $\mathcal{O}(\alpha)$ corrections around the distribution peaks amount to about 5% and about 10% for the electron and muon channel, respectively, while higher-order effects vary from 0.2% to 0.5%.

Program	$\sigma^{\rm tot}$ [nb]: WITH CUTS		
	Born	$\mathcal{O}(\alpha)$	Best
$W^- \longrightarrow e^-\bar{\nu}_e$			
HORACE	3.23633 (12)	3.18707 (13)	3.18696 (13)
WINHAC	3.23629 (09)	3.18779 (07)	3.18765 (06)
$\delta = (\mathrm{W}-\mathrm{H})/\mathrm{W}$	$-1.2\,(4.6)\times 10^{-5}$	$2.3\,(0.5)\times 10^{-4}$	$2.2\,(0.5)\times 10^{-4}$
$W^- \longrightarrow \mu^-\bar{\nu}_\mu$			
HORACE	3.23632 (12)	3.15990 (12)	3.16013 (13)
WINHAC	3.23630 (07)	3.16418 (06)	3.16409 (05)
$\delta = (\mathrm{W}-\mathrm{H})/\mathrm{W}$	$-0.6\,(4.3)\times 10^{-5}$	$1.35\,(0.05)\times 10^{-3}$	$1.25\,(0.05)\times 10^{-3}$
$W^+ \longrightarrow e^+\nu_e$			
HORACE	4.39341 (16)	4.32186 (17)	4.32187 (18)
WINHAC	4.39328 (13)	4.32286 (10)	4.32273 (08)
$\delta = (\mathrm{W}-\mathrm{H})/\mathrm{W}$	$-3.0\,(4.7)\times 10^{-5}$	$2.3\,(0.5)\times 10^{-4}$	$2.0\,(0.5)\times 10^{-4}$
$W^+ \longrightarrow \mu^+\nu_\mu$			
HORACE	4.39340 (16)	4.28255 (16)	4.28326 (16)
WINHAC	4.39336 (10)	4.28837 (08)	4.28848 (08)
$\delta = (\mathrm{W}-\mathrm{H})/\mathrm{W}$	$-0.9\,(4.3)\times 10^{-5}$	$1.36\,(0.05)\times 10^{-3}$	$1.22\,(0.05)\times 10^{-3}$

Table 3: The hadron-level results for the Born, the $\mathcal{O}(\alpha)$ and the "Best"-level total cross section (in nb) from HORACE and WINHAC with cuts. The numbers in parentheses are statistical errors for the last digits.

5 Quark-mass effects

In this section we present the effects of using non-zero quark masses in the hadron-level W-production process for various observables. In our test we used the following quark masses:

$$\begin{aligned} &m_u = 0.003\,\mathrm{GeV}, \quad m_d = 0.00675\,\mathrm{GeV}, \quad m_s = 0.1175\,\mathrm{GeV} \\ &m_c = 1.2\,\mathrm{GeV}, \qquad m_b = 4.25\,\mathrm{GeV}. \end{aligned} \tag{5}$$

All other input parameters were the same as in the previous section.

In the case of non-zero quark masses, there is an ambiguity in defining the quark four-momentum q in terms of proton momentum p and the Bjorken x-variable. Some of the possible definitions are:

1. the "energy-like scheme" : $q^0 = xp^0$;
2. the "momentum-like scheme": $q^3 = xp^3$;
3. the "light-cone-like scheme": $q^+ = xp^+$, where $a^+ = (a^0 + a^3)/\sqrt{2}$.

All the above definitions are equivalent for zero quark masses.

In the following figures we compare the distributions presented in the previous section for zero quark masses with the corresponding ones obtained using non-zero quark masses.

The Figures 29–32 show the size of the quark-mass effect for the "energy-like scheme", Figs. 33–36 for the "momentum-like scheme", and Figs. 37–40 for the "light-cone-like scheme". It is worth noticing that the size and also the sign of the quark-mass effects significantly depend on the scheme adopted. For example, in the "energy-like scheme" the quark-mass effects are of the order of $+2\%$ around the peaks of the transverse mass and lepton transverse momentum distributions, while in the "momentum-like" scheme the corrections are of the same order but of opposite sign, amounting to about -3%. These considerations about the different sign of the effects predicted by the above two schemes do apply to the W rapidity and lepton pseudorapidity, even if for such distributions the effect is confined at the few per mille level. The smallest effects due to non-zero quark masses is observed for all the considered distributions in the "light-cone-like" scheme. An appropriate inclusion of non-zero quark mass effects should therefore be carefully considered in view of future improved measurements of the W-boson mass and width at hadron colliders.

6 Summary and outlook

We presented a number of tuned comparisons between the predictions of two recently developed event generators, HORACE and WINHAC for single-W-boson production at hadron colliders. This is important in view of future precision determinations of the W-boson mass and width, as well as for PDFs and parton-luminosity measurements.

Both generators include $\mathcal{O}(\alpha)$ and higher-order QED corrections to leptonic W decays, according to different and independent formulations. The comparisons were performed both at the parton level with fixed quarks-beam energy and at the hadron level for proton–proton collisions at the LHC. To understand the source of possible discrepancies, the comparisons were carried out at three different levels of theoretical precision: Born, $\mathcal{O}(\alpha)$ and with higher-order effects. Both integrated cross sections and differential distributions were examined. The agreement between the two programs for the main single-W-boson observables is satisfactory. The higher-order QED corrections, although based on two quite different approaches, numerically agree very well. These comparisons indicate that both HORACE and WINHAC describe the QED effects in leptonic W-boson decays with the precision that is sufficient for the W-boson mass and width determination as well as the PDFs and parton luminosities measurements at the LHC. Of course, neither of the programs includes all the effects that are necessary for the full experimental data analysis; however, they are good starting points for further developments.

The next step would be to see how various QED effects and differences between the programs translate into fitted values of the W mass and width and the actual determination of the PDFs and parton luminosities. A first evaluation of the impact of higher-order QED corrections to the W mass extraction, from a fit to the transverse-mass distribution, has been performed in Ref. [5]. A more realistic analysis should, however, be made in close connection with the actual experimental procedures.

Further tests should also include the complete $\mathcal{O}(\alpha)$ EW corrections for single-W-

boson production, and, last but not least, the QCD effects, which are crucial for any precise measurement at the LHC.

In last section, we show how the inclusion of non-zero quark masses may affect the main single-W-boson observables at the LHC. Both the size and shape of these effects depend on the scheme adopted for dealing with massive-quarks kinematics. Particularly large effects are seen in the distributions of the W-boson transverse mass and the charge lepton transverse momentum. Therefore, the proper treatment of quark masses in theoretical descriptions of the respective processes can be of importance for the precision measurement of the W mass and width at the LHC.

We plan to carry out similar studies for proton–antiproton collisions at the Tevatron.

Acknowledgements

Two of us (S.J. and W.P.) acknowledge the kind support of the CERN TH Unit, Physics Department.

References

[1] G. Altarelli and M. Mangano, editors, *Proceedings of the Workshop on Standard Model Physics (and More) at the LHC* (CERN 2000-004, Geneva, 2000).

[2] S. Jadach, Electroweak tools for the LHC, cf. [4], available at: http://agenda.cern.ch/fullAgenda.php?ida=a031522.

[3] M. Dittmar, F. Pauss and D. Zurcher, Phys. Rev. **D56**, 7284 (1997), hep-ex/9705004.

[4] N. Brook *et al.*, CERN Workshop on Monte Carlo Tools for the LHC, CERN, July 7 – August 1, 2003, http://mlm.home.cern.ch/mlm/mcwshop03/mcwshop.html.

[5] C. Carloni Calame, G. Montagna, O. Nicrosini and M. Treccani, Higher-order QED corrections to W-boson mass determination at hadron colliders, preprint FNT/T 2003/05; hep-ph/0303102, to appear in Phys. Rev. **D**.

[6] W. Płaczek and S. Jadach, WINHAC 1.13: The Monte Carlo Event Generator for Single W-Boson Production with Leptonic Decays in Hadron Collisions, available from http://cern.ch/placzek.

[7] U. Baur, S. Keller and D. Wackeroth, Phys. Rev. **D59**, 013002 (1998).

[8] C. Carloni Calame, C. Lunardini, G. Montagna, O. Nicrosini and F. Piccinini, Nucl. Phys. **B584**, 459 (2000).

[9] C. Carloni Calame, Phys. Lett. **B520**, 16 (2001).

[10] F. Berends and R. Kleiss, Z. Phys. **C27**, 365 (1985).

[11] H. Plothow-Besch, PDFLIB: Proton, pion and photon parton density functions, parton density functions of the nucleus, the α_s calculations, H.Plothow-Besch/CERN-ETT/TT, 2000.04.17.

[12] W. Płaczek and S. Jadach, Eur. Phys. J. **C29**, 325 (2003), hep-ph/0302065.

[13] D. Bardin *et al.*, $\mathcal{O}(\alpha)$ electroweak form factors for W-boson decays, 2003, private communications.

[14] S. Jadach, Comput. Phys. Commun. **152**, 55 (2003), physics/0203033.

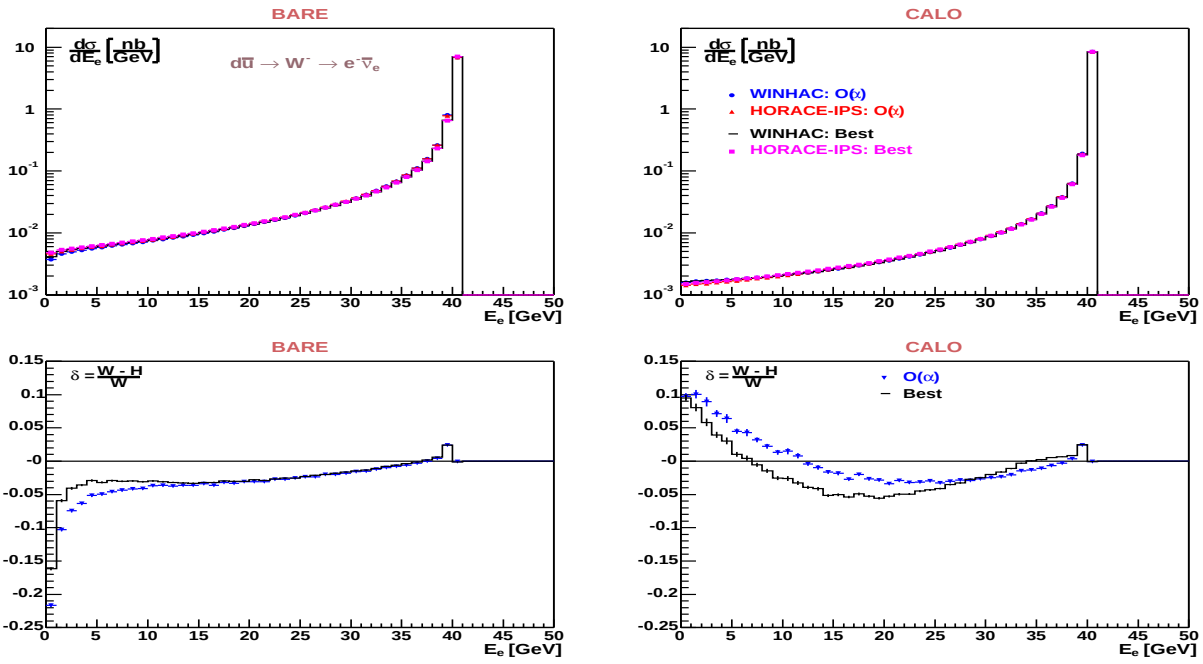

Figure 1: Distributions of the electron energy at parton level for $\mathcal{O}(\alpha)$ and "Best" predictions from HORACE and WINHAC, as well as their differences. The results are shown for BARE (left) and CALO (right) event selections.

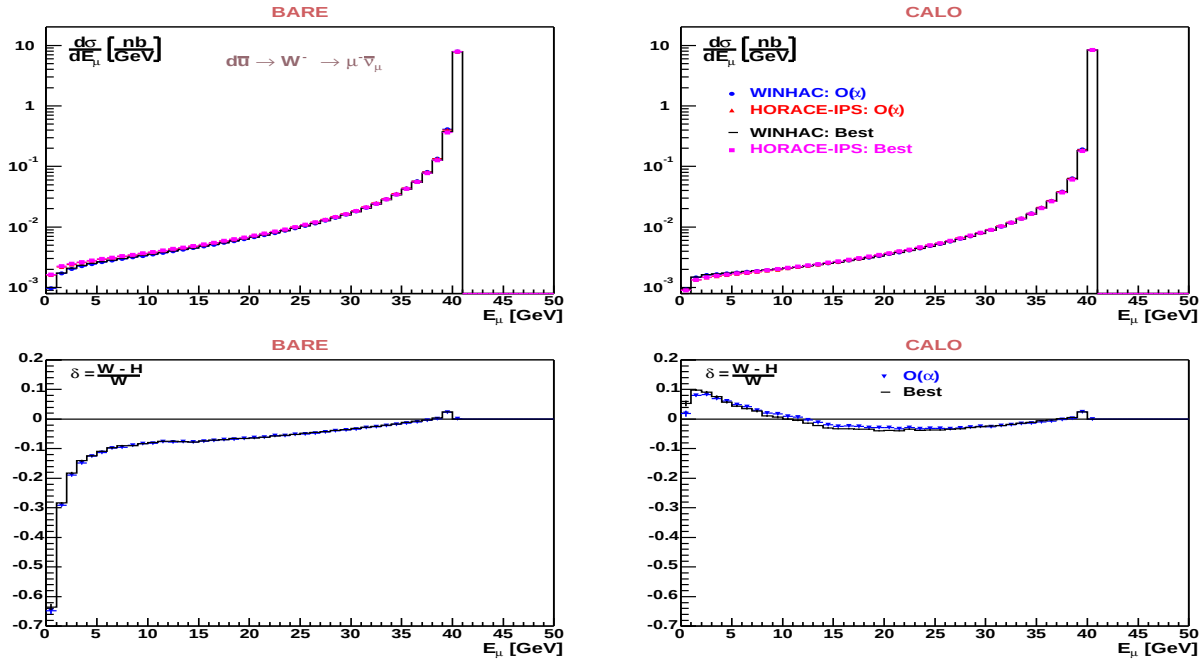

Figure 2: Distributions of the muon energy at parton level for $\mathcal{O}(\alpha)$ and "Best" predictions from HORACE and WINHAC, as well as their differences. The results are shown for BARE (left) and CALO (right) event selections.

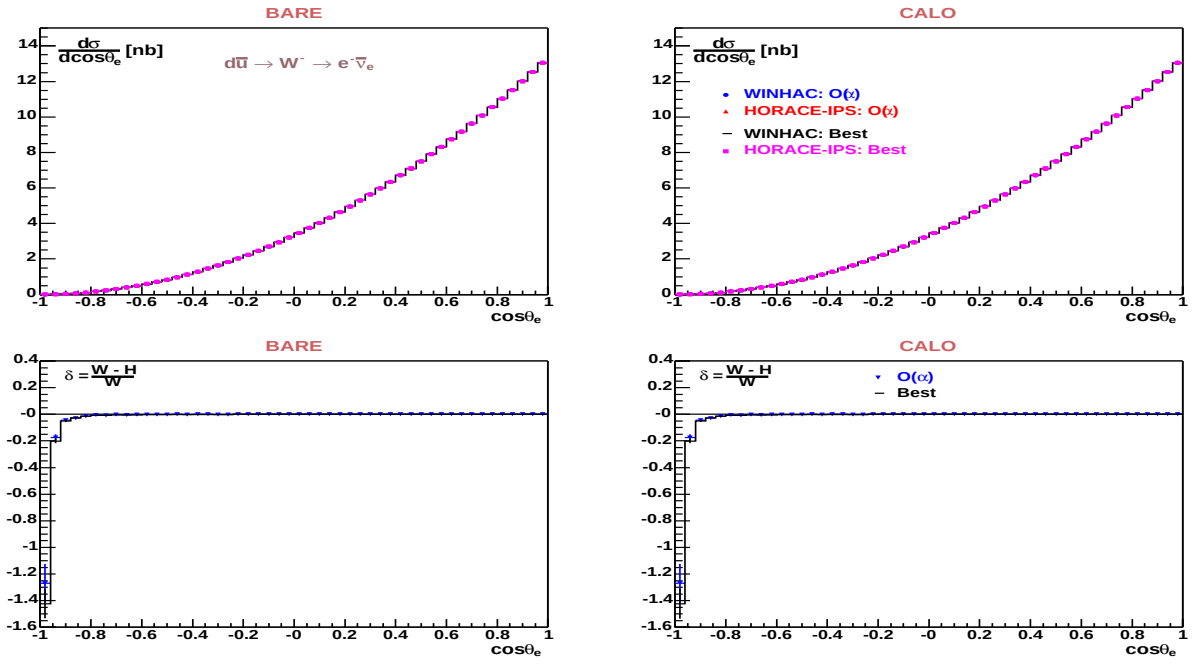

Figure 3: Distributions of the electron polar angle at parton level for $\mathcal{O}(\alpha)$ and "Best" predictions from HORACE and WINHAC, as well as their differences. The results are shown for BARE (left) and CALO (right) event selections.

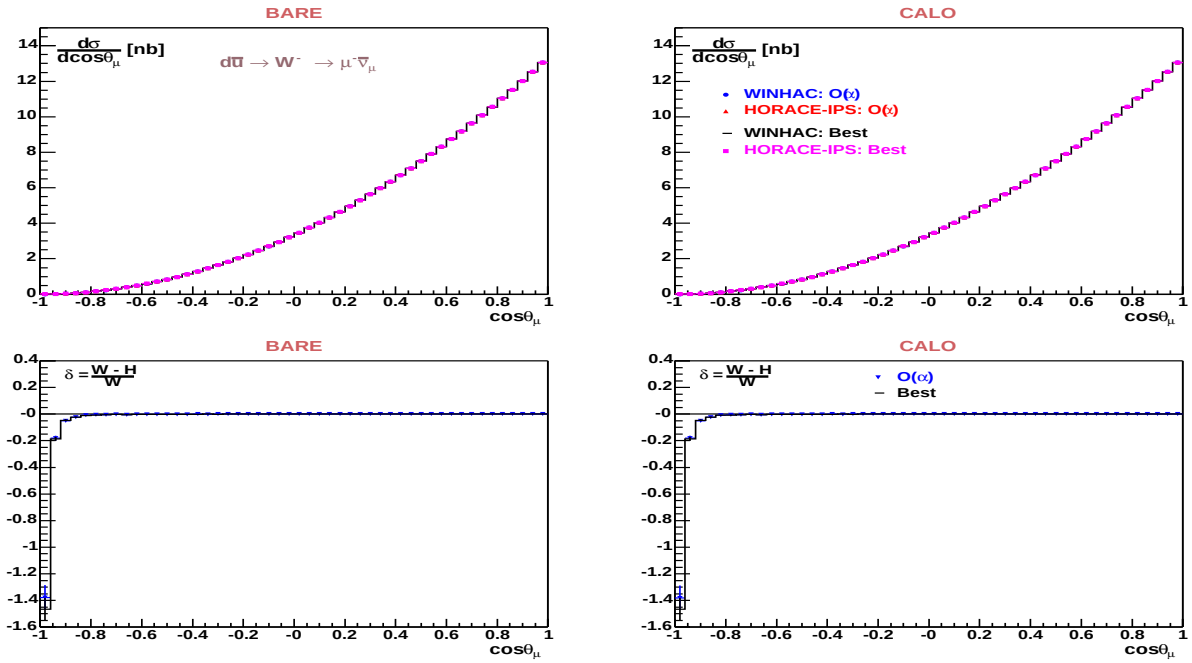

Figure 4: Distributions of the muon polar angle at parton level for $\mathcal{O}(\alpha)$ and "Best" predictions from HORACE and WINHAC, as well as their differences. The results are shown for BARE (left) and CALO (right) event selections.

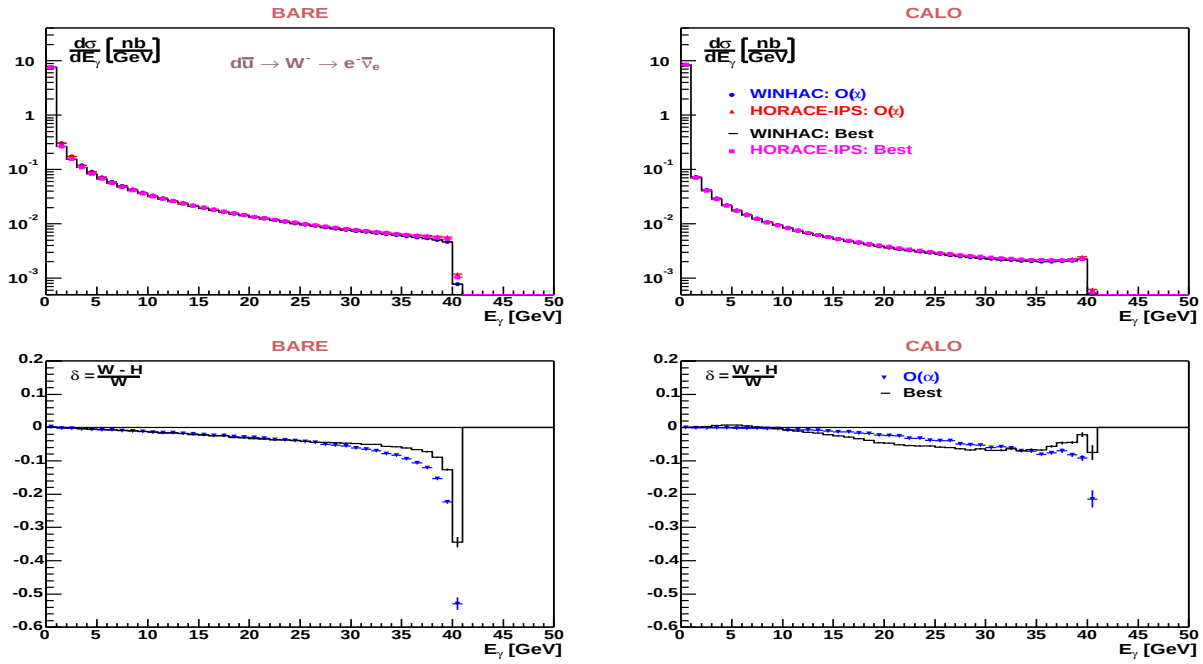

Figure 5: Distributions of the hardest-photon energy at parton level in the electron channel for $\mathcal{O}(\alpha)$ and "Best" predictions from HORACE and WINHAC, as well as their differences. The results are shown for BARE (left) and CALO (right) event selections.

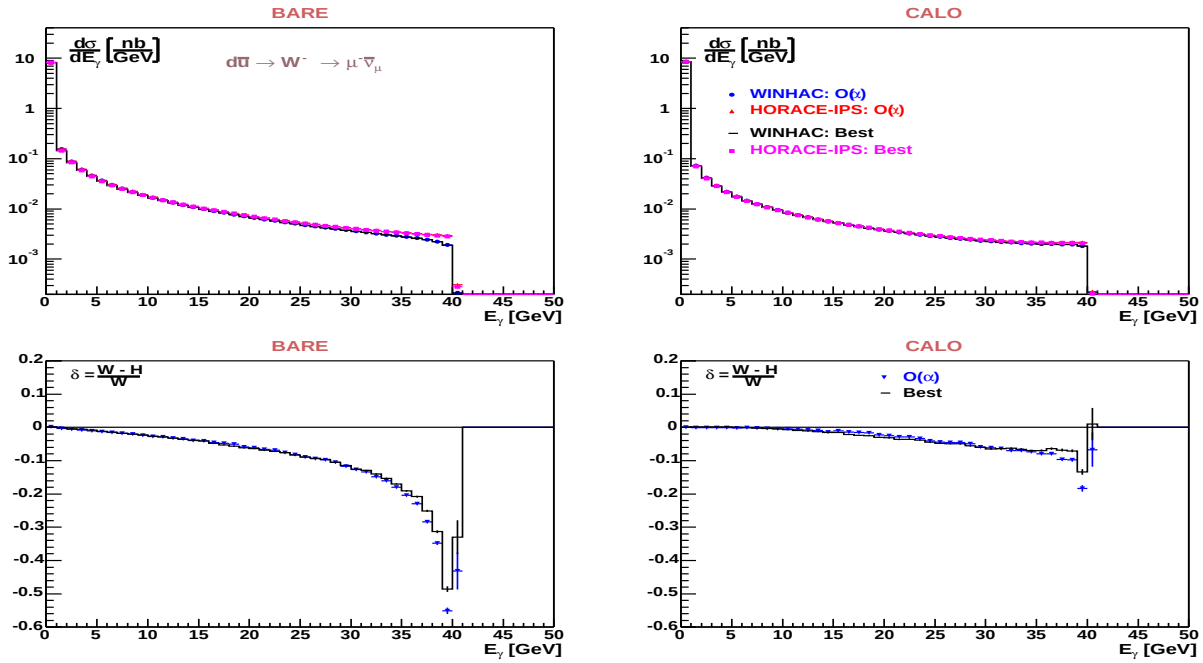

Figure 6: Distributions of the hardest-photon energy at parton level in the muon channel for $\mathcal{O}(\alpha)$ and "Best" predictions from HORACE and WINHAC, as well as their differences. The results are shown for BARE (left) and CALO (right) event selections.

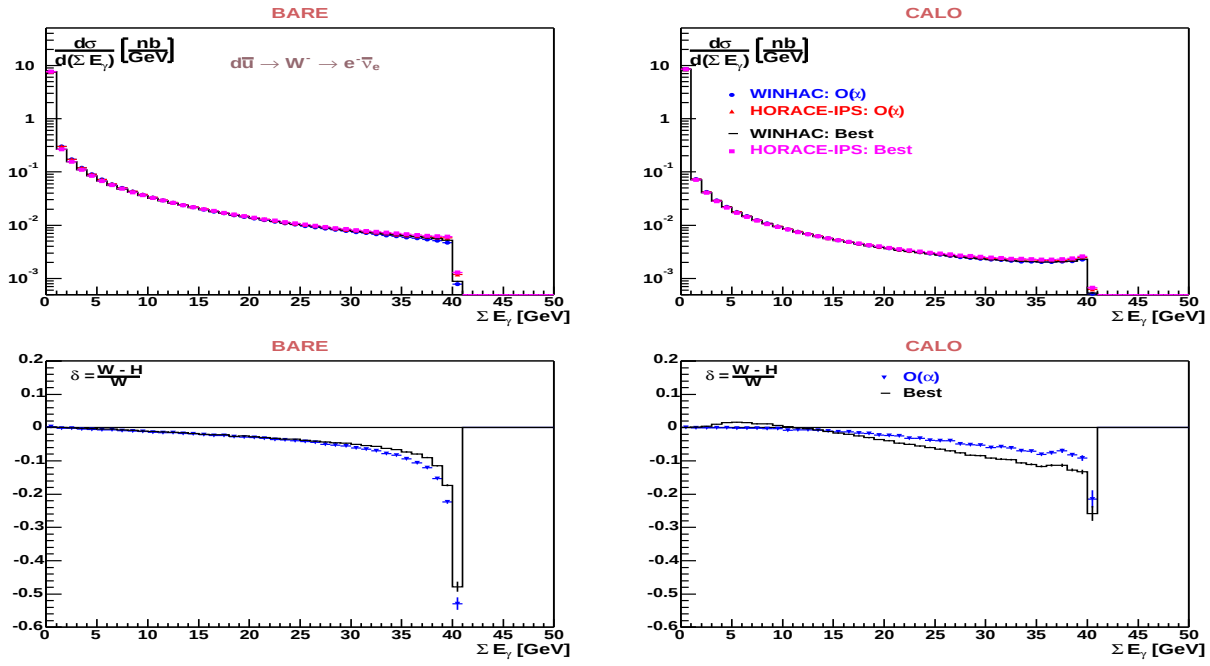

Figure 7: Distributions of the total energy radiated by photons in the electron channel for $\mathcal{O}(\alpha)$ and "Best" predictions from HORACE and WINHAC, as well as their differences. The results are shown for BARE (left) and CALO (right) event selections.

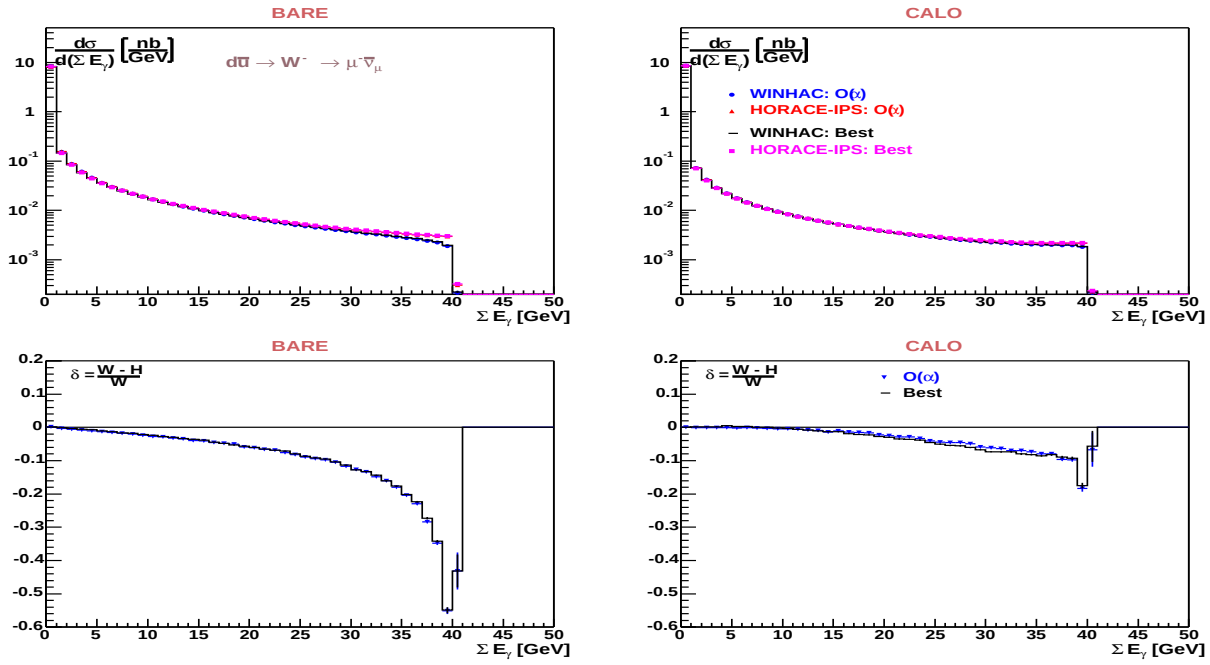

Figure 8: Distributions of the total energy radiated by photons in the muon channel for $\mathcal{O}(\alpha)$ and "Best" predictions from HORACE and WINHAC, as well as their differences. The results are shown for BARE (left) and CALO (right) event selections.

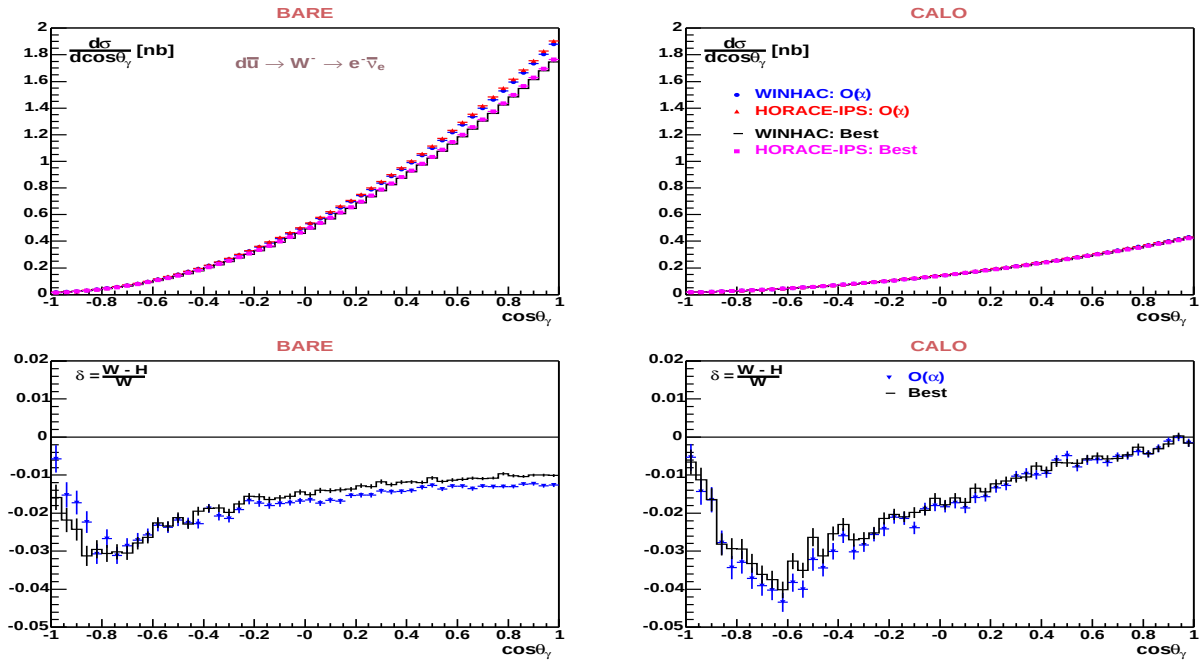

Figure 9: Distributions of the hardest-photon polar angle in the electron channel for $\mathcal{O}(\alpha)$ and "Best" predictions from HORACE and WINHAC, as well as their differences. The results are shown for BARE (left) and CALO (right) event selections.

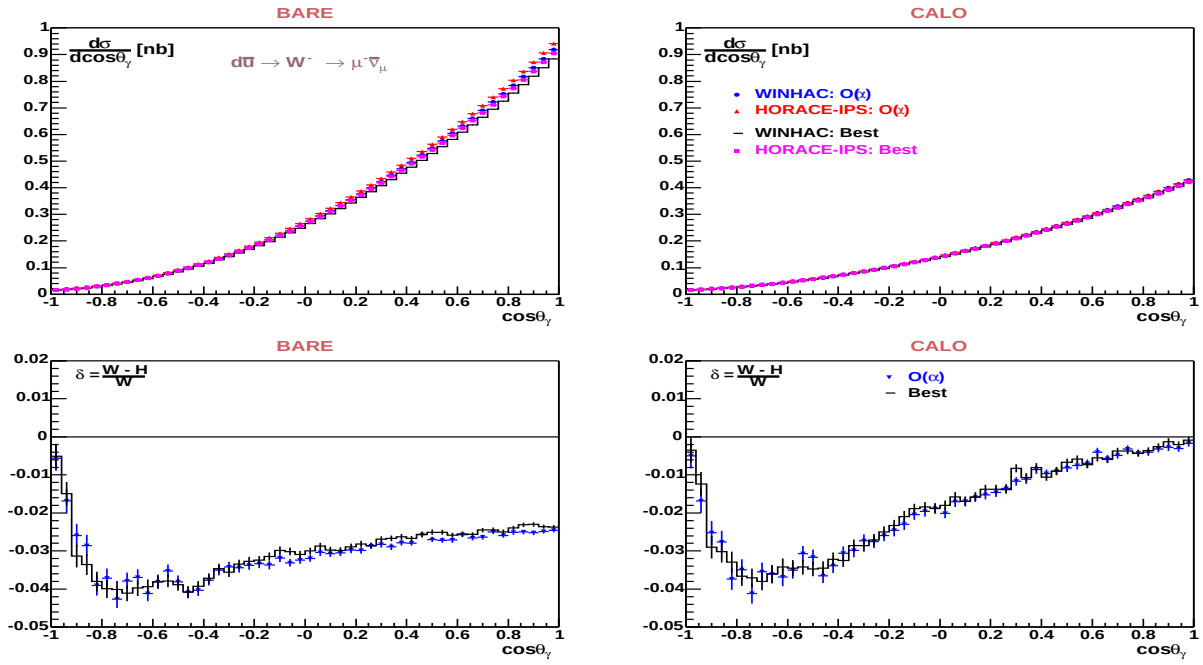

Figure 10: Distributions of the hardest-photon polar angle in the muon channel for $\mathcal{O}(\alpha)$ and "Best" predictions from HORACE and WINHAC, as well as their differences. The results are shown for BARE (left) and CALO (right) event selections.

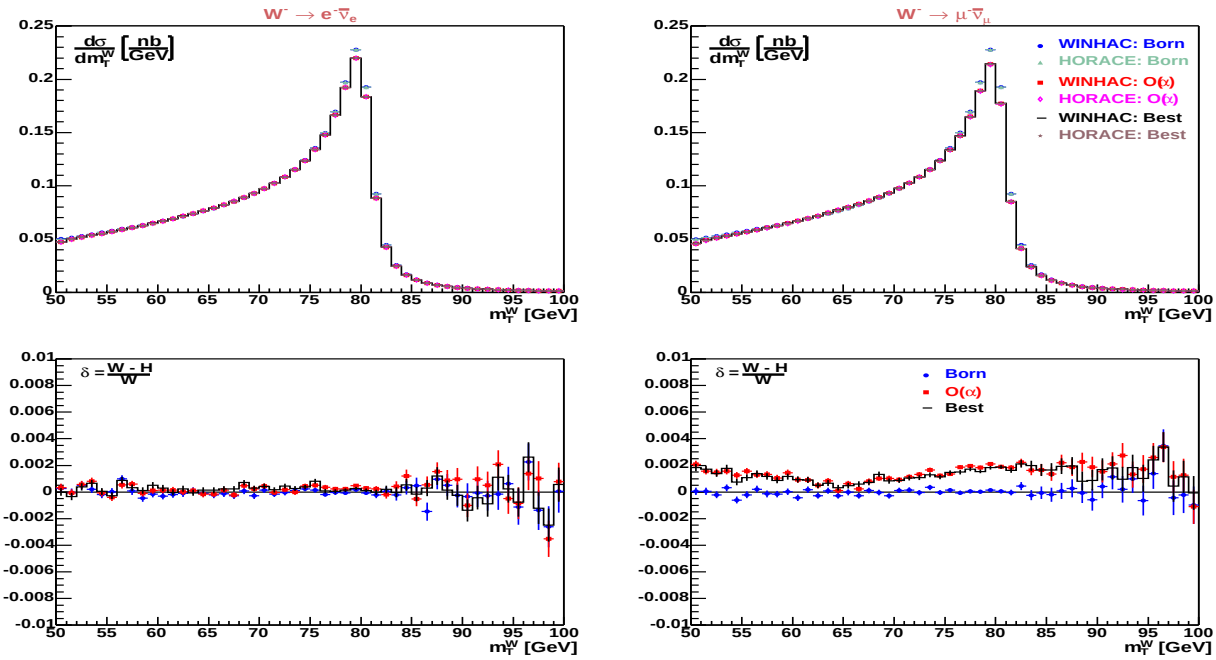

Figure 11: Distributions of the W^- transverse mass at hadron level for Born, $\mathcal{O}(\alpha)$ and "Best" predictions from HORACE and WINHAC, as well as their differences. The results are shown for the electron (left) and muon (right) channels.

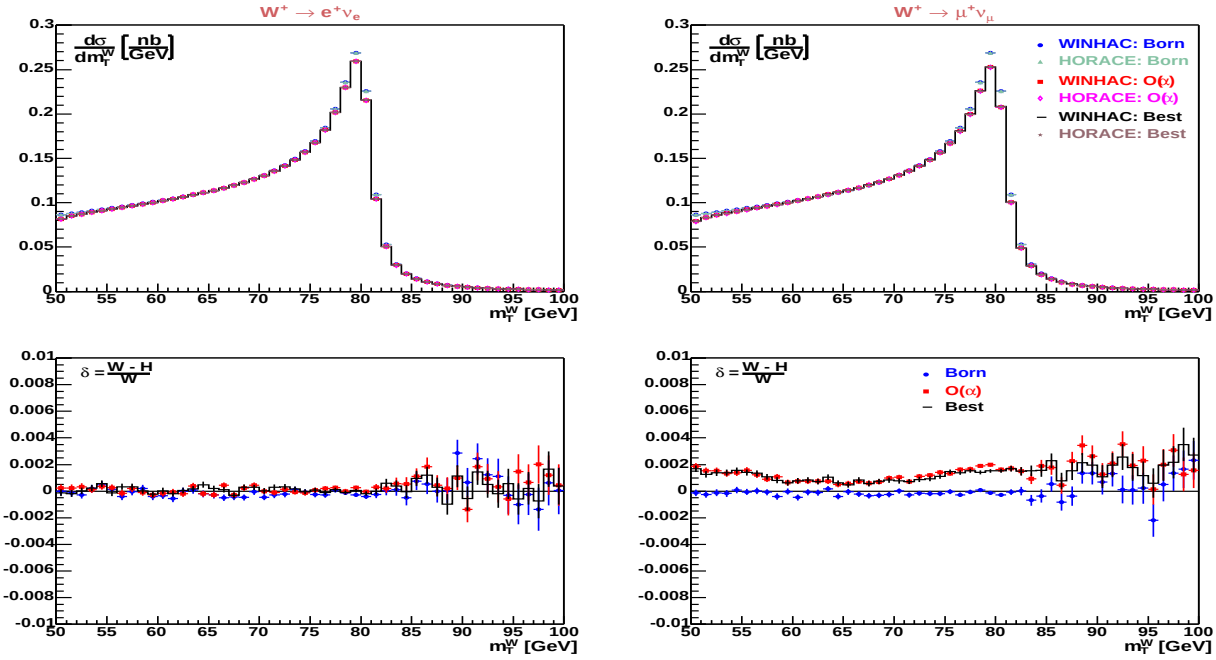

Figure 12: Distributions of the W^+ transverse mass at hadron level for Born, $\mathcal{O}(\alpha)$ and "Best" predictions from HORACE and WINHAC, as well as their differences. The results are shown for the electron (left) and muon (right) channels.

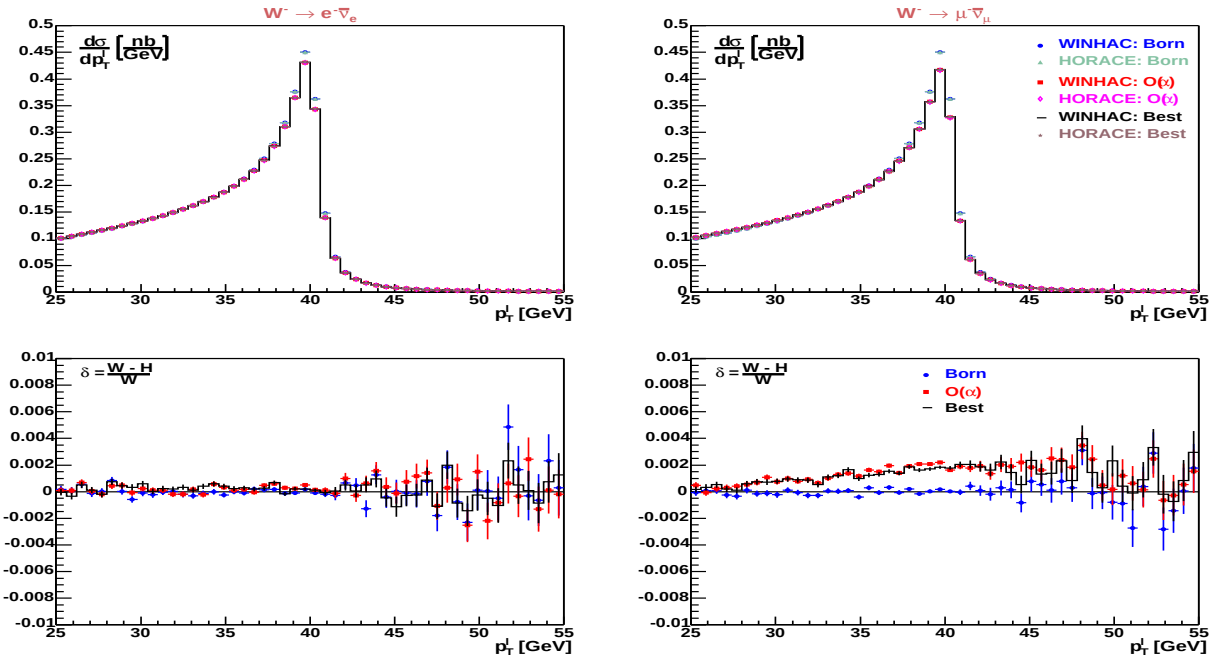

Figure 13: Distributions of the charged lepton transverse momentum at hadron level for Born, $\mathcal{O}(\alpha)$ and "Best" predictions of W^- production from HORACE and WINHAC, as well as their differences. The results are shown for the electron (left) and muon (right) channels.

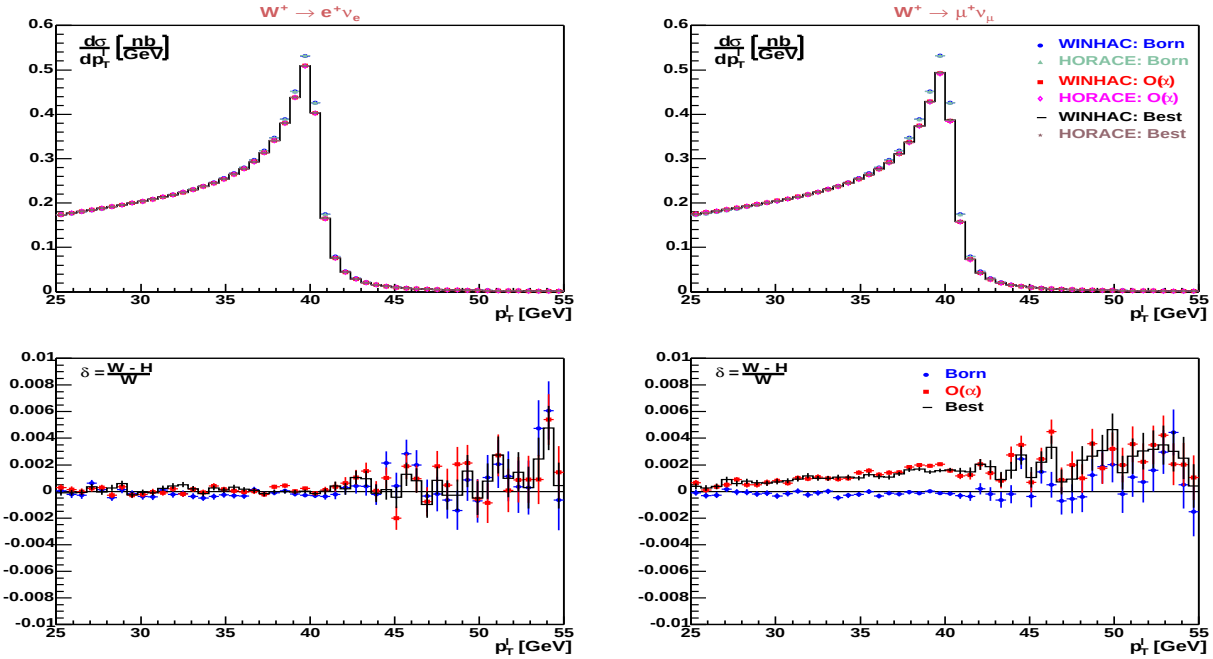

Figure 14: Distributions of the charged lepton transverse momentum at hadron level for Born, $\mathcal{O}(\alpha)$ and "Best" predictions of W^+ production from HORACE and WINHAC, as well as their differences. The results are shown for the electron (left) and muon (right) channels.

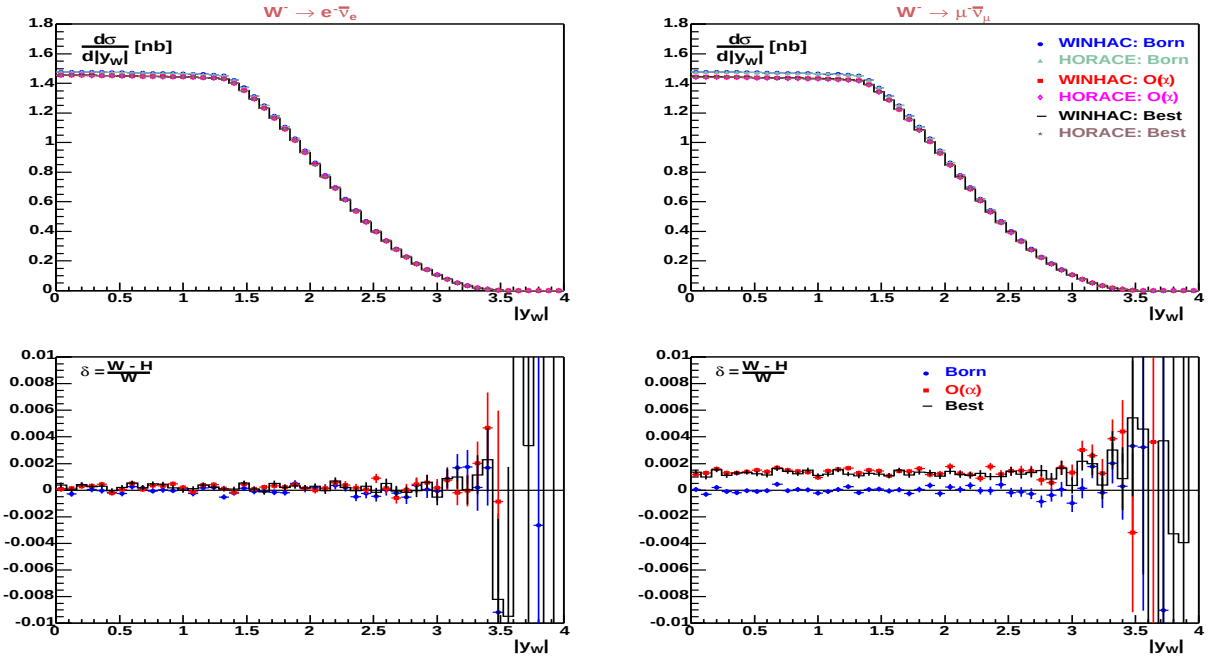

Figure 15: Distributions of the W^- rapidity at hadron level for Born, $\mathcal{O}(\alpha)$ and "Best" predictions from HORACE and WINHAC, as well as their differences. The results are shown for the electron (left) and muon (right) channels.

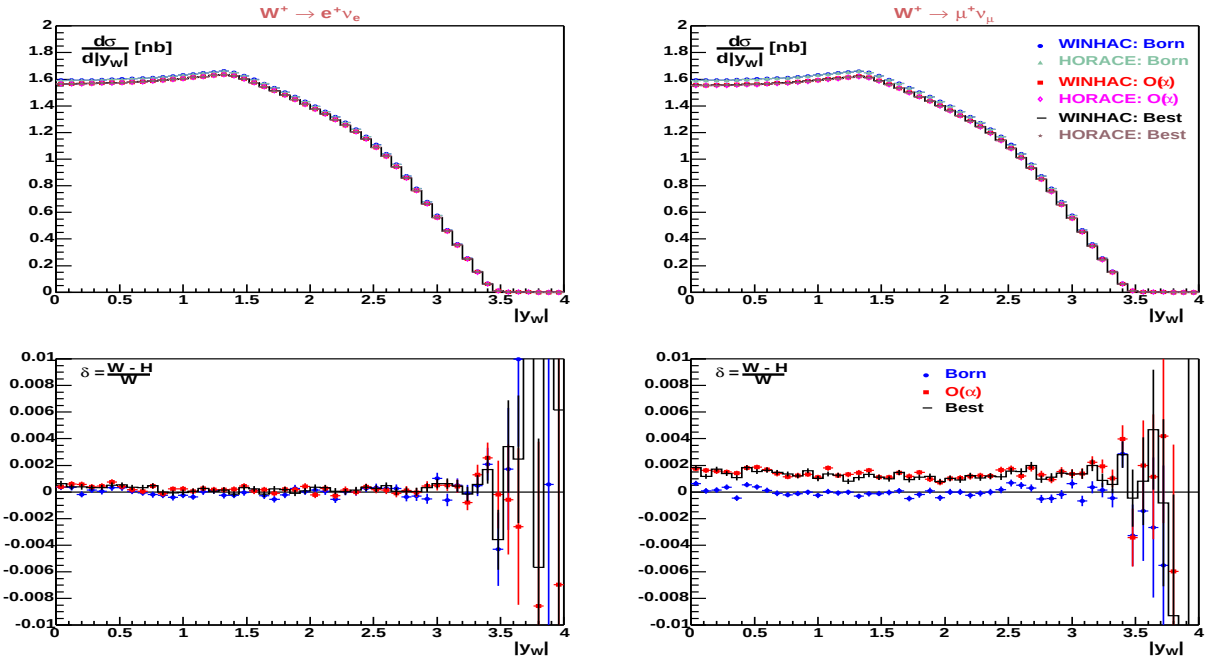

Figure 16: Distributions of the W^+ rapidity at hadron level for Born, $\mathcal{O}(\alpha)$ and "Best" predictions from HORACE and WINHAC, as well as their differences. The results are shown for the electron (left) and muon (right) channels.

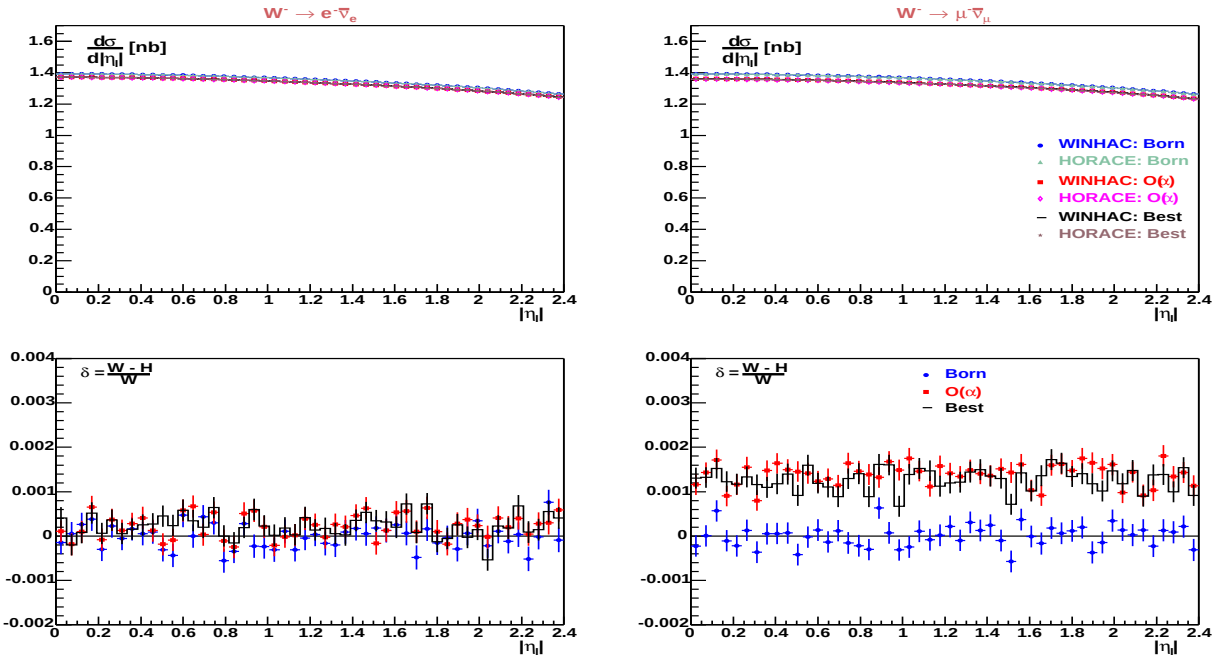

Figure 17: Distributions of the charged lepton pseudorapidity at hadron level for Born, $\mathcal{O}(\alpha)$ and "Best" predictions of W^- production from HORACE and WINHAC, as well as their differences. The results are shown for the electron (left) and muon (right) channels.

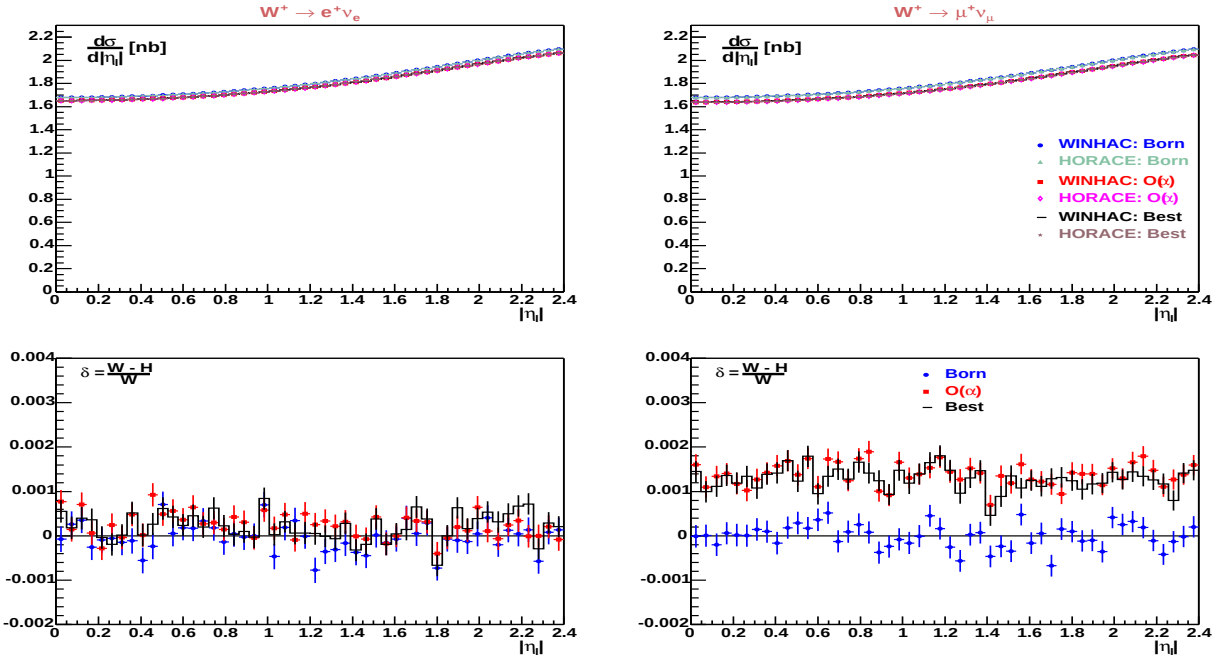

Figure 18: Distributions of the charged lepton pseudorapidity at hadron level for Born, $\mathcal{O}(\alpha)$ and "Best" predictions of W^+ production from HORACE and WINHAC, as well as their differences. The results are shown for the electron (left) and muon (right) channels.

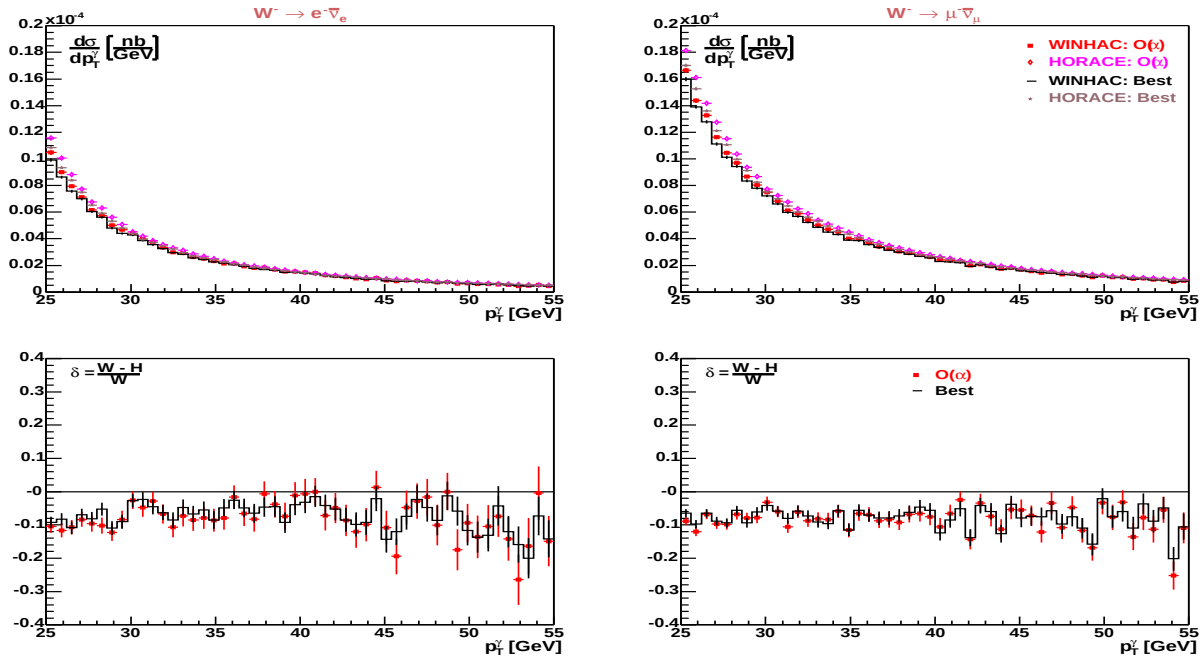

Figure 19: Distributions of the hardest-photon transverse momentum at hadron level for $\mathcal{O}(\alpha)$ and "Best" predictions of W^- production from HORACE and WINHAC, as well as their differences. The results are shown for the electron (left) and muon (right) channels.

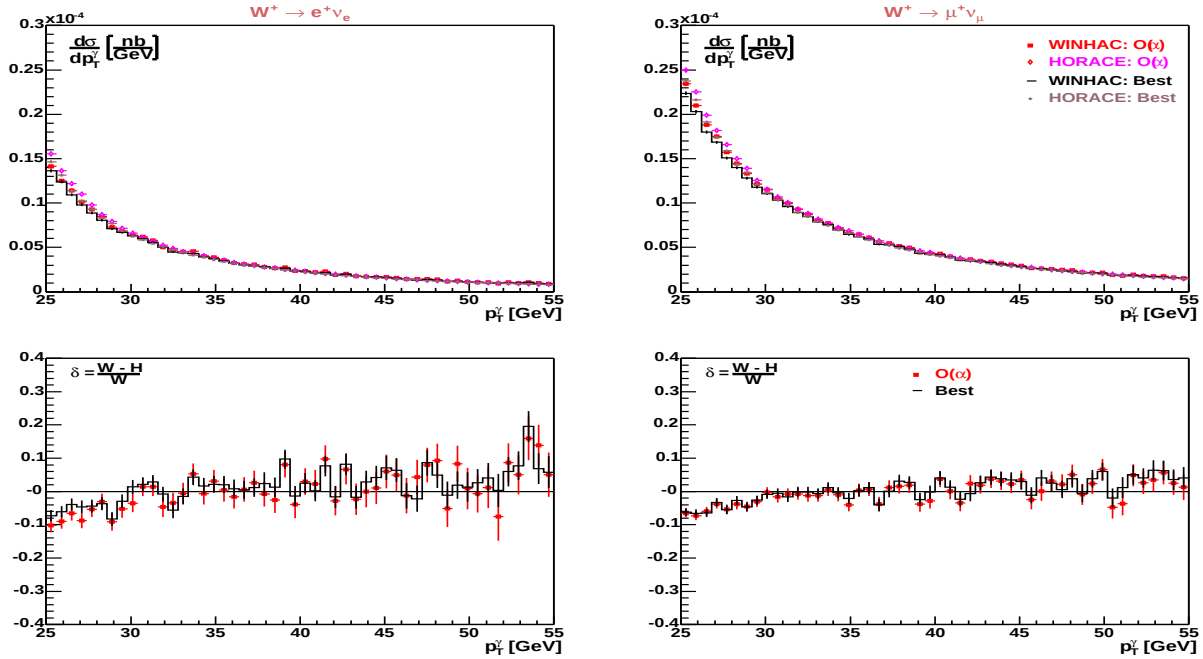

Figure 20: Distributions of the hardest-photon transverse momentum at hadron level for $\mathcal{O}(\alpha)$ and "Best" predictions of W^+ production from HORACE and WINHAC, as well as their differences. The results are shown for the electron (left) and muon (right) channels.

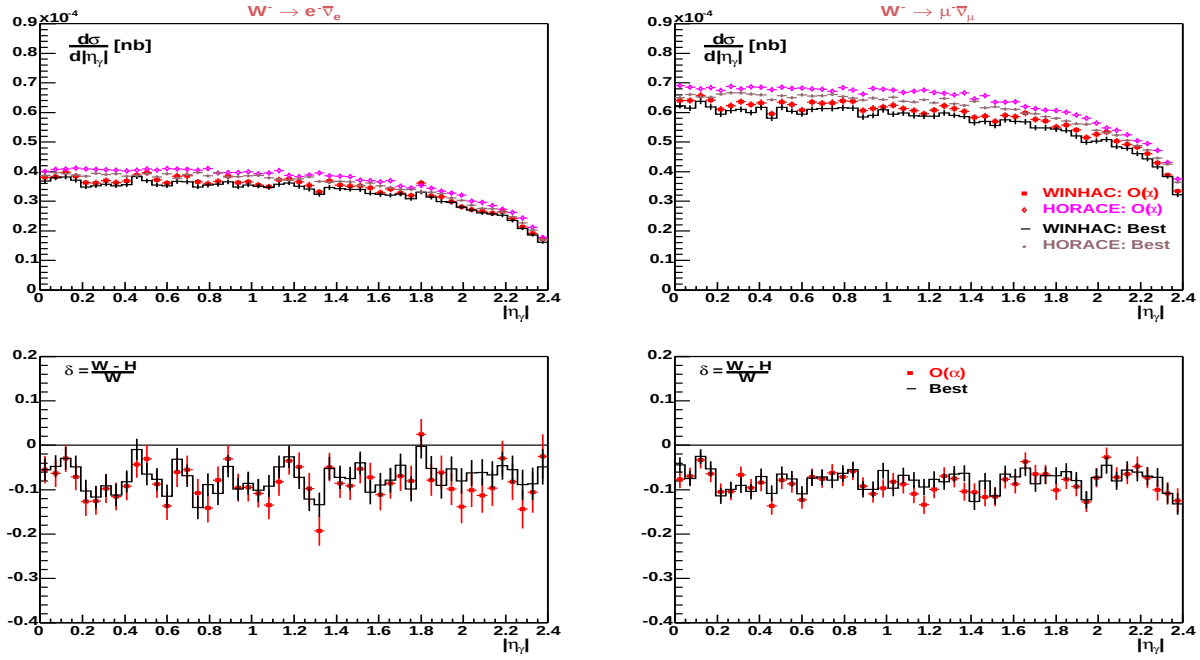

Figure 21: Distributions of the hardest-photon pseudorapidity at hadron level for $\mathcal{O}(\alpha)$ and "Best" predictions of W^- production from HORACE and WINHAC, as well as their differences. The results are shown for the electron (left) and muon (right) channels.

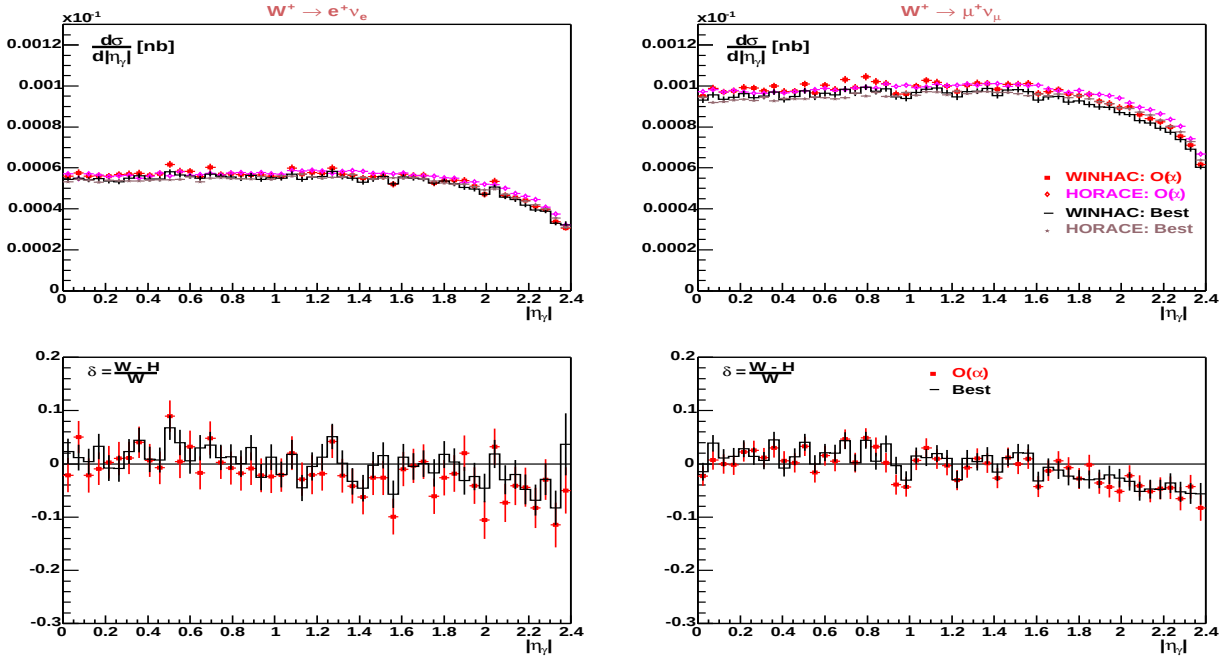

Figure 22: Distributions of the hardest-photon pseudorapidity at hadron level for $\mathcal{O}(\alpha)$ and "Best" predictions of W^+ production from HORACE and WINHAC, as well as their differences. The results are shown for the electron (left) and muon (right) channels.

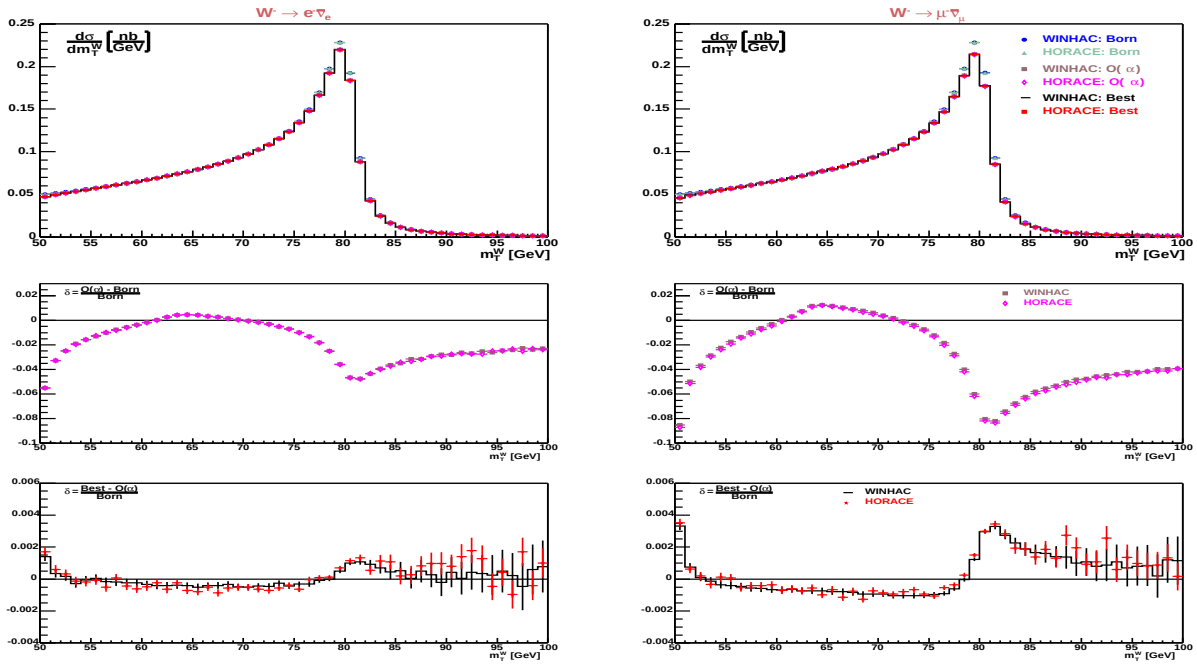

Figure 23: Distributions of the W^- transverse mass at hadron level for Born, $\mathcal{O}(\alpha)$ and "Best" predictions from HORACE and WINHAC, and the size of QED corrections. The results are shown for the electron (left) and muon (right) channels.

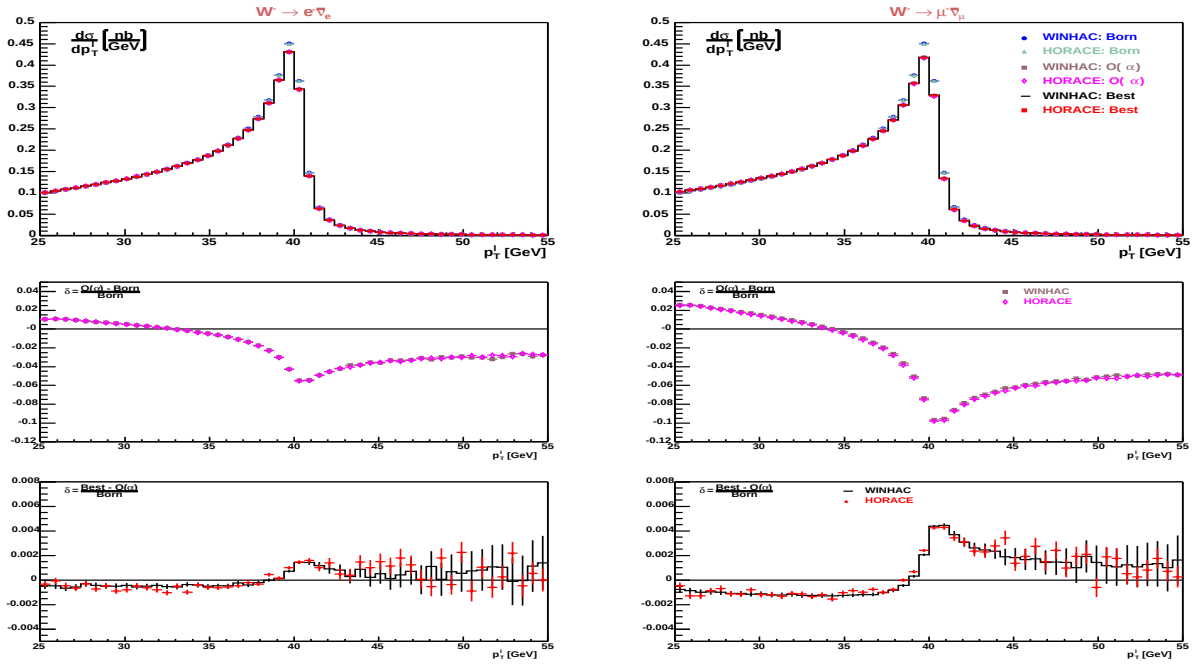

Figure 24: Distributions of the charged lepton transverse momentum at hadron level for Born, $\mathcal{O}(\alpha)$ and "Best" predictions of W^- production from HORACE and WINHAC, and the size of QED corrections. The results are shown for the electron (left) and muon (right) channels.

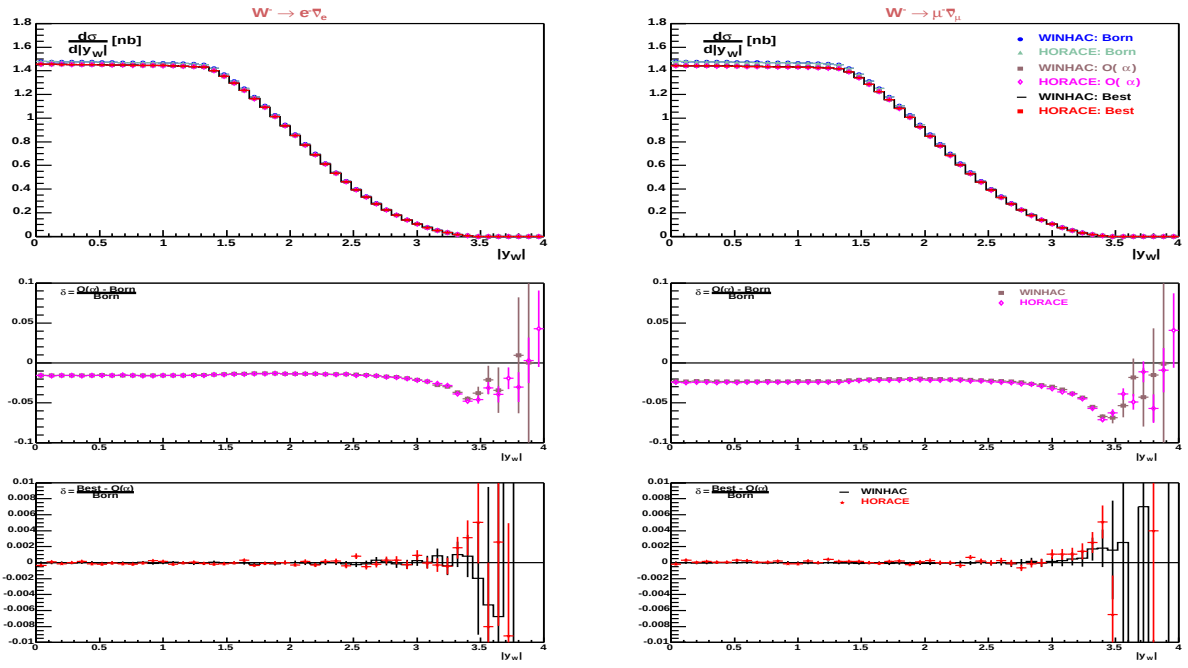

Figure 25: Distributions of the W^- rapidity at hadron level for Born, $\mathcal{O}(\alpha)$ and "Best" predictions from HORACE and WINHAC, and the size of QED corrections. The results are shown for the electron (left) and muon (right) channels.

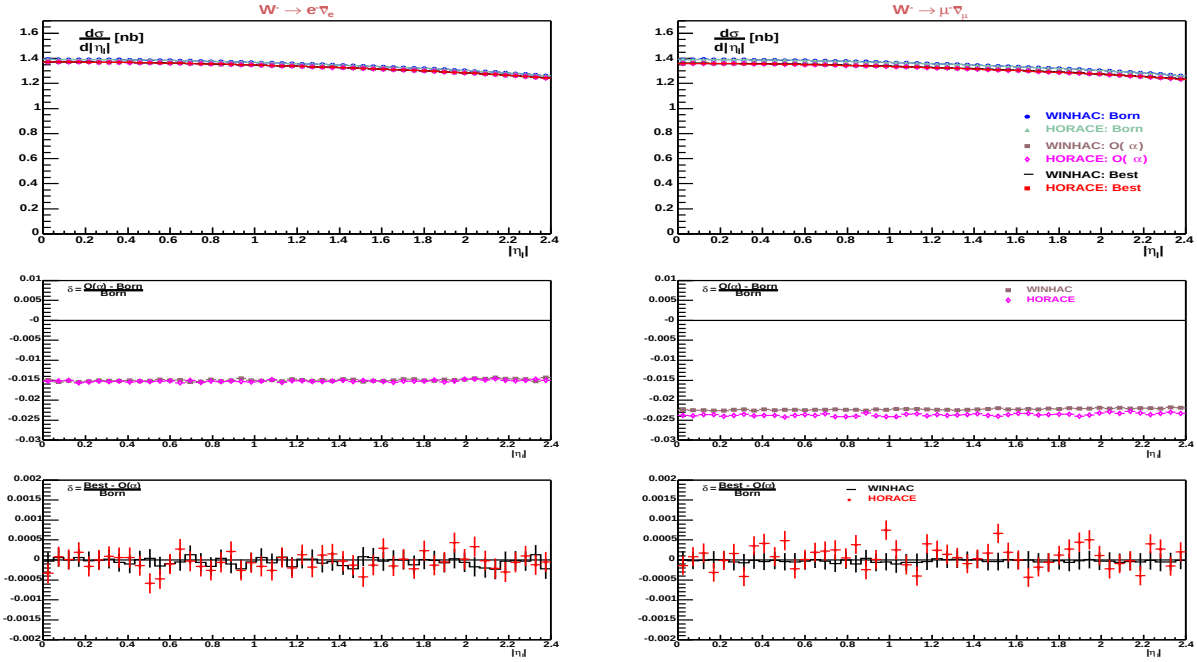

Figure 26: Distributions of the charged lepton pseudorapidity at hadron level for Born, $\mathcal{O}(\alpha)$ and "Best" predictions of W^- production from HORACE and WINHAC, and the size of QED corrections. The results are shown for the electron (left) and muon (right) channels.

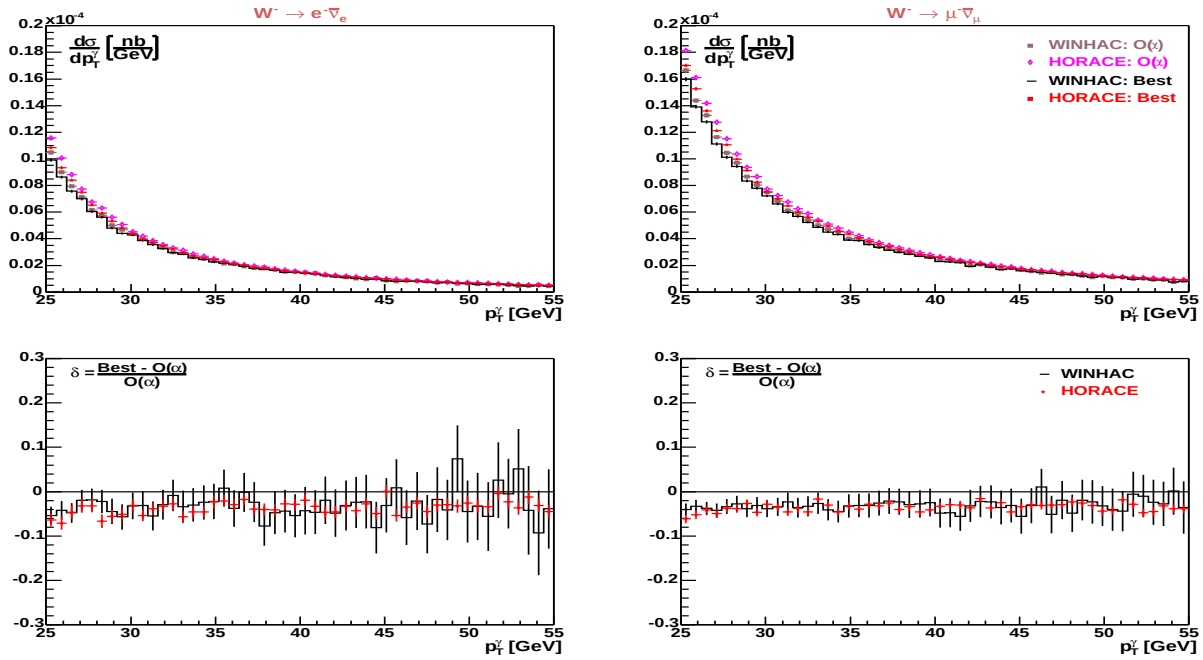

Figure 27: Distributions of the hardest-photon transverse momentum at hadron level for $\mathcal{O}(\alpha)$ and "Best" predictions of W^- production from HORACE and WINHAC, and the size of QED corrections. The results are shown for the electron (left) and muon (right) channels.

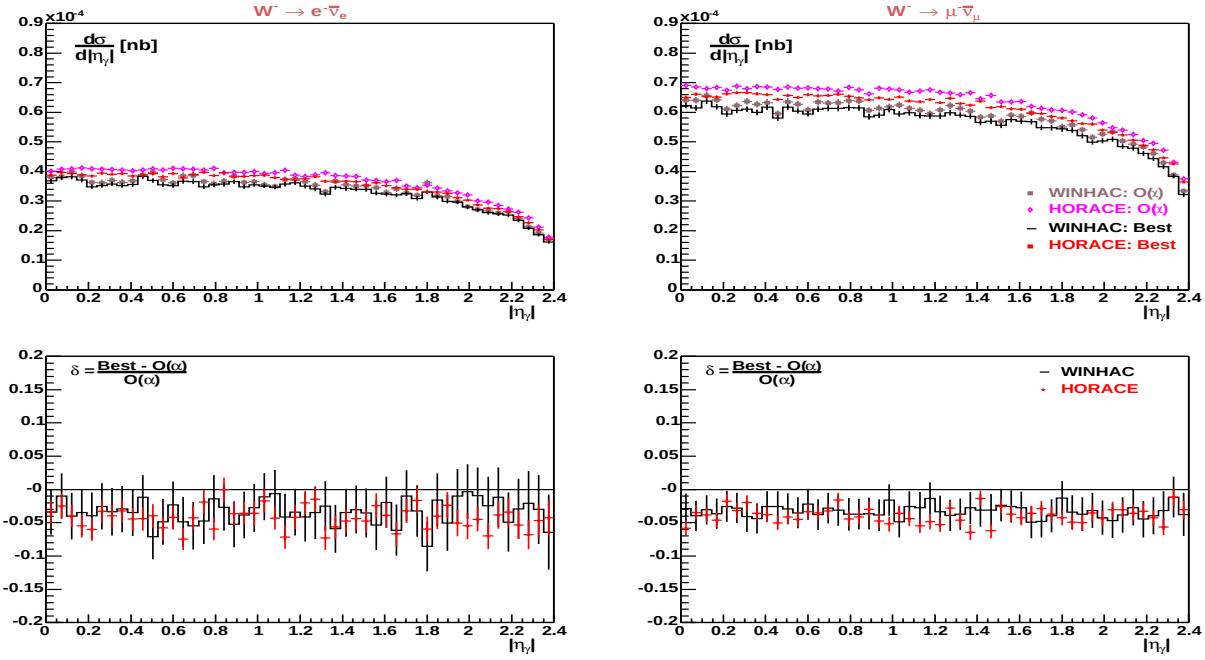

Figure 28: Distributions of the hardest-photon pseudorapidity at hadron level $\mathcal{O}(\alpha)$ and "Best" predictions of W^- production from HORACE and WINHAC, and the size of QED corrections. The results are shown for the electron (left) and muon (right) channels.

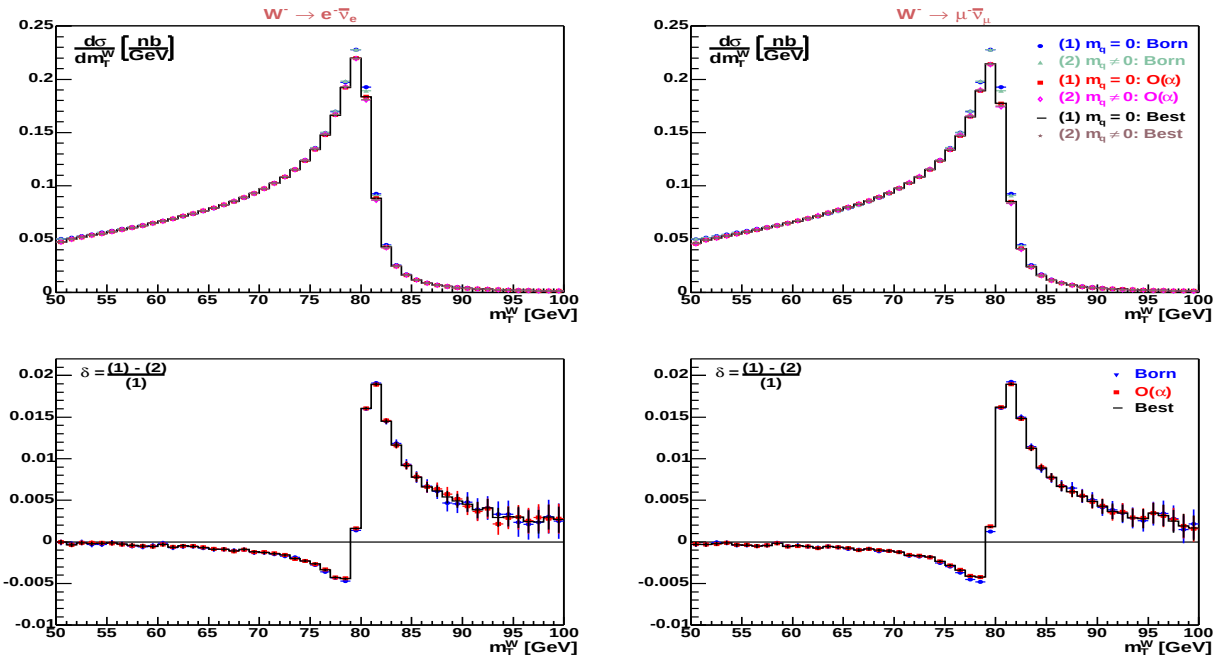

Figure 29: The quark-mass effects in the "energy-like scheme" for the W^- transverse mass distribution at the Born, $\mathcal{O}(\alpha)$ and "Best" levels, obtained from WINHAC. The results are shown for the electron (left) and muon (right) channels.

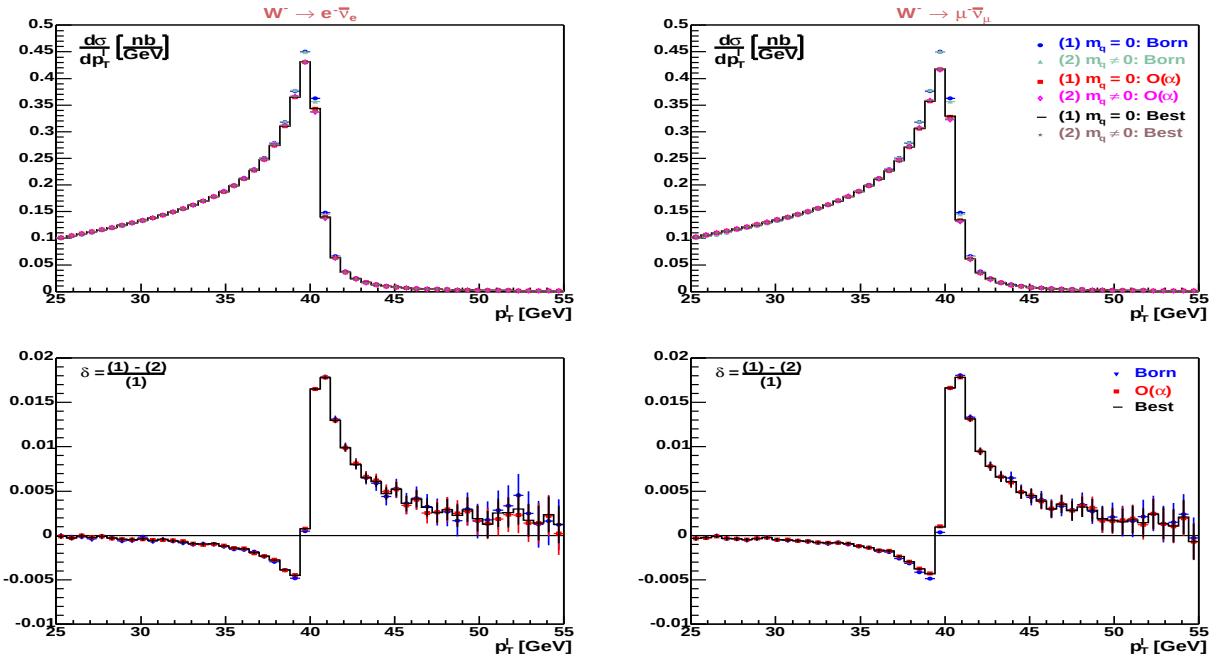

Figure 30: The quark-mass effects in the "energy-like scheme" for the charged lepton transverse momentum distribution of W^- production at the Born, $\mathcal{O}(\alpha)$ and "Best" levels, obtained from WINHAC. The results are shown for the electron (left) and muon (right) channels.

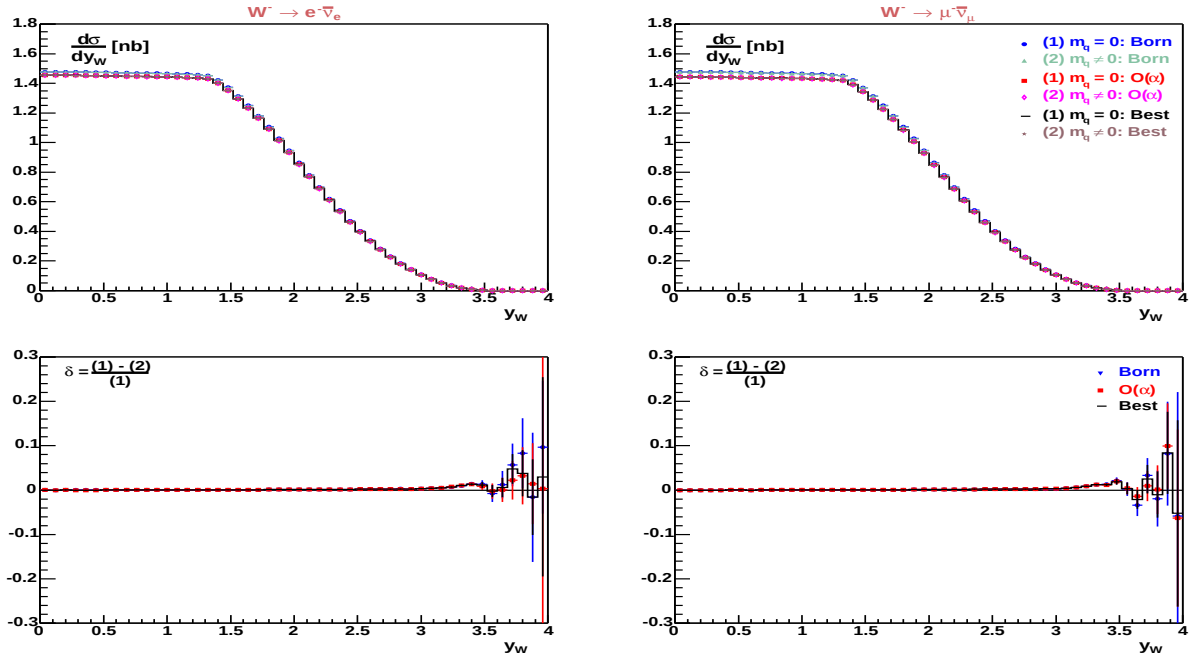

Figure 31: The quark-mass effects in the "energy-like scheme" for the W^- rapidity distribution at the Born, $\mathcal{O}(\alpha)$ and "Best" levels, obtained from WINHAC. The results are shown for the electron (left) and muon (right) channels.

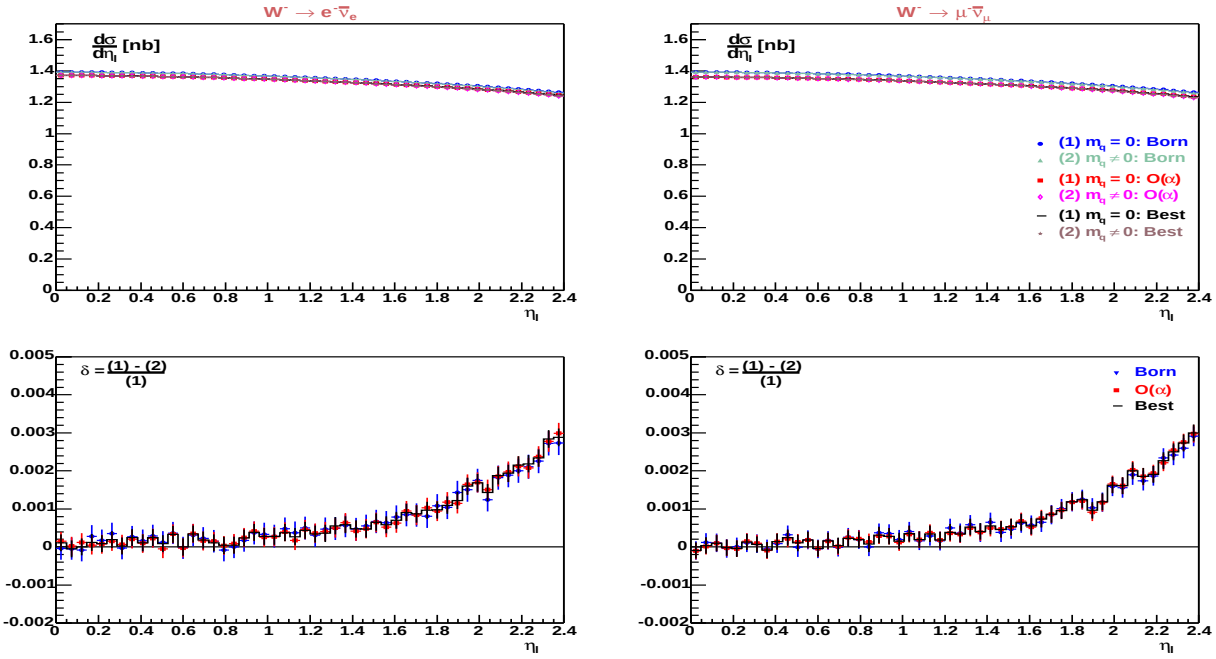

Figure 32: The quark-mass effects in the "energy-like scheme" for the charged lepton pseudorapidity distribution of W^- production at the Born, $\mathcal{O}(\alpha)$ and "Best" levels, obtained from WINHAC. The results are shown for the electron (left) and muon (right) channels.

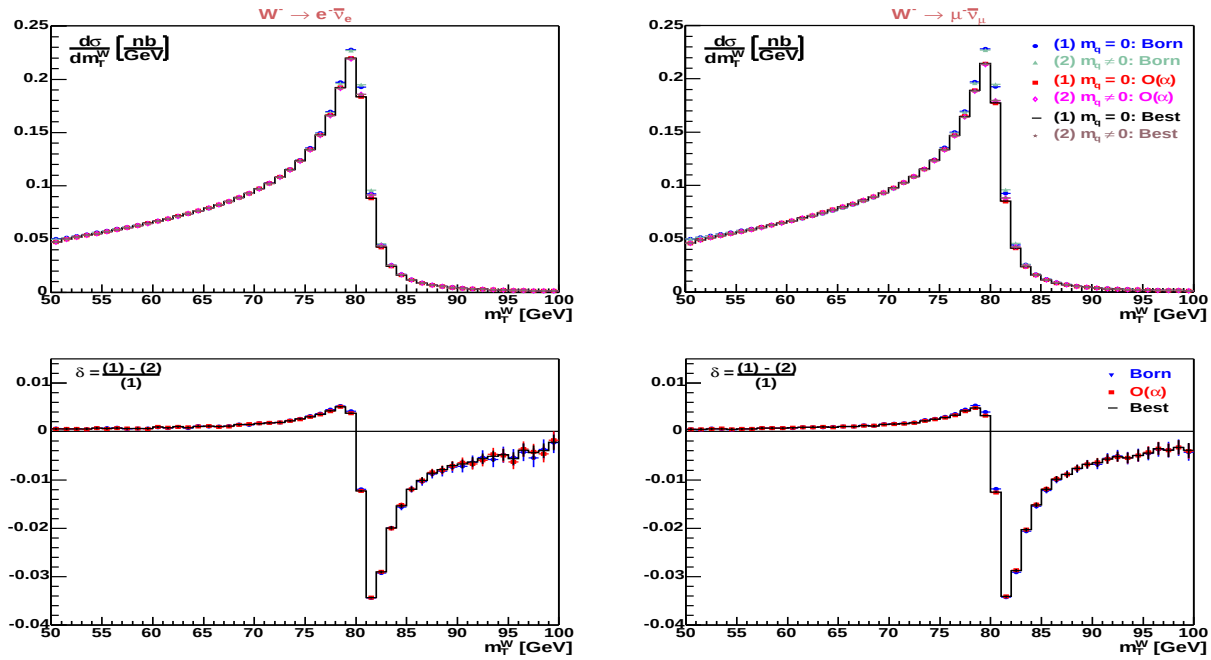

Figure 33: The quark-mass effects in the "momentum-like scheme" for the W^- transverse mass distribution at the Born, $\mathcal{O}(\alpha)$ and "Best" levels, obtained from WINHAC. The results are shown for the electron (left) and muon (right) channels.

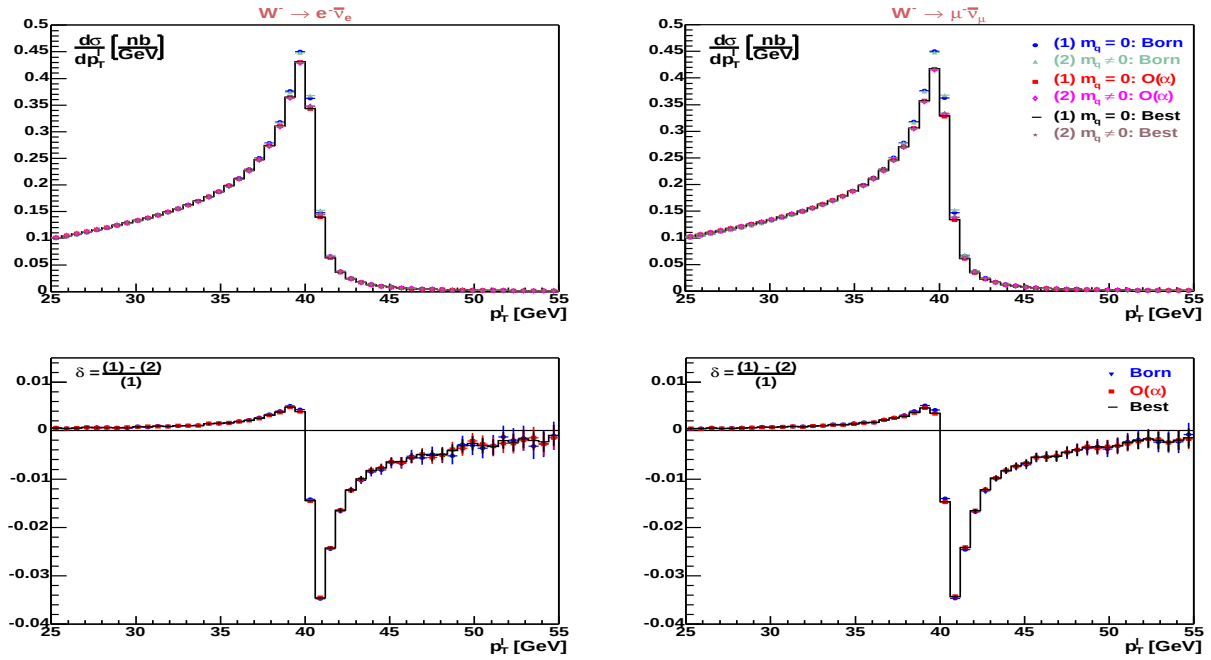

Figure 34: The quark-mass effects in the "momentum-like scheme" for the charged lepton transverse momentum distribution of W^- production at the Born, $\mathcal{O}(\alpha)$ and "Best" levels, obtained from WINHAC. The results are shown for the electron (left) and muon (right) channels.

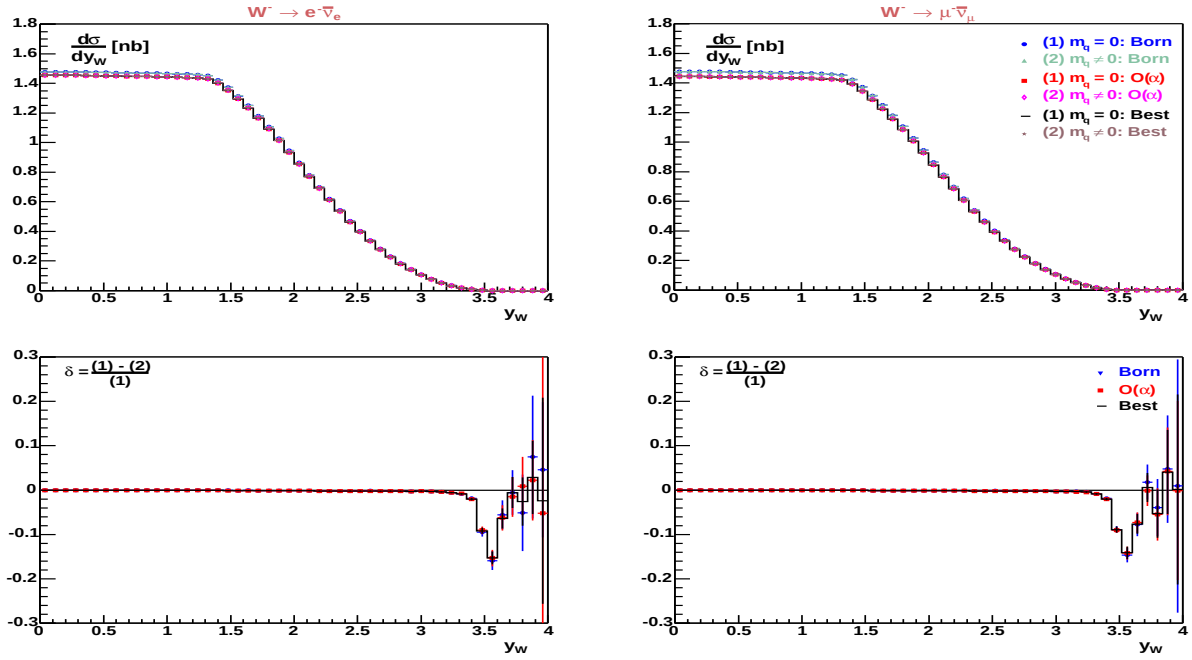

Figure 35: The quark-mass effects in the "momentum-like scheme" for the W^- rapidity distribution at the Born, $\mathcal{O}(\alpha)$ and "Best" levels, obtained from WINHAC. The results are shown for the electron (left) and muon (right) channels.

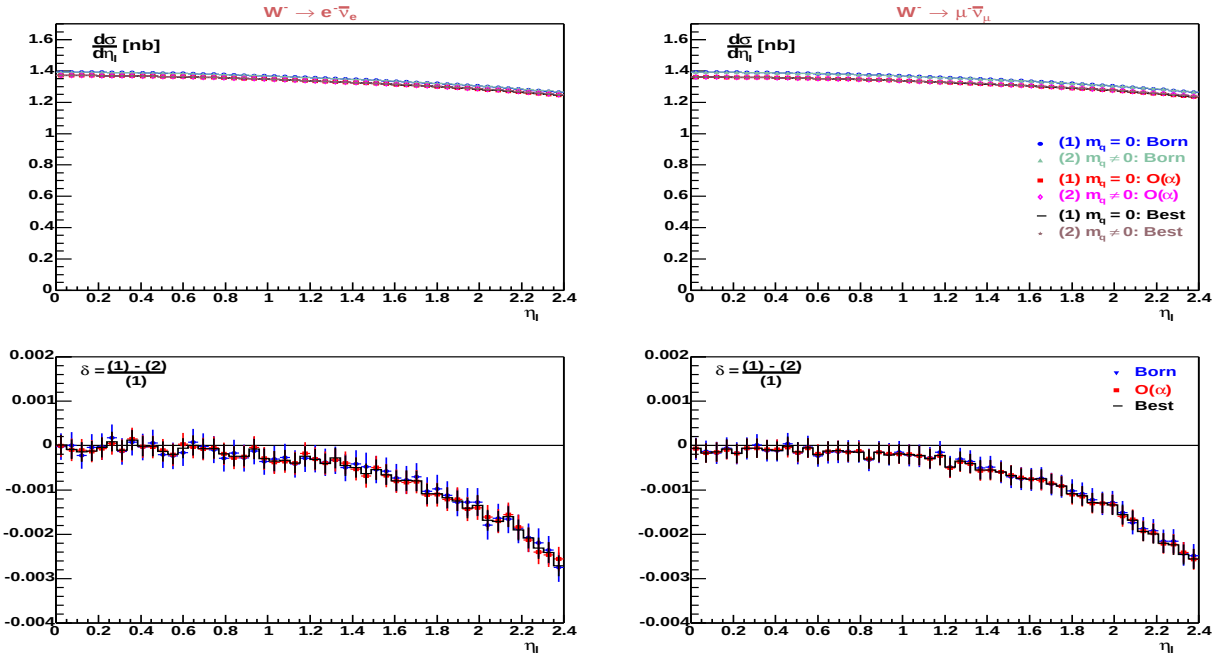

Figure 36: The quark-mass effects in the "momentum-like scheme" for the charged lepton pseudorapidity distribution of W^- production at the Born, $\mathcal{O}(\alpha)$ and "Best" levels, obtained from WINHAC. The results are shown for the electron (left) and muon (right) channels.

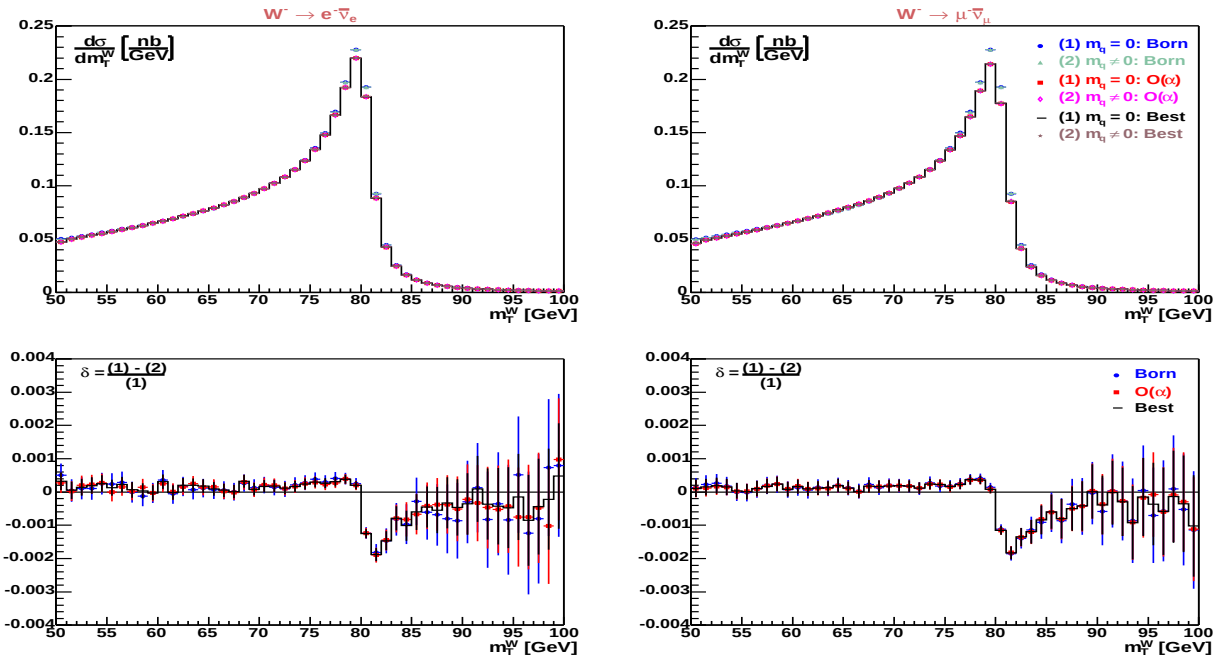

Figure 37: The quark-mass effects in the "light-cone-like scheme" for the W^- transverse mass distribution at the Born, $\mathcal{O}(\alpha)$ and "Best" levels, obtained from WINHAC. The results are shown for the electron (left) and muon (right) channels.

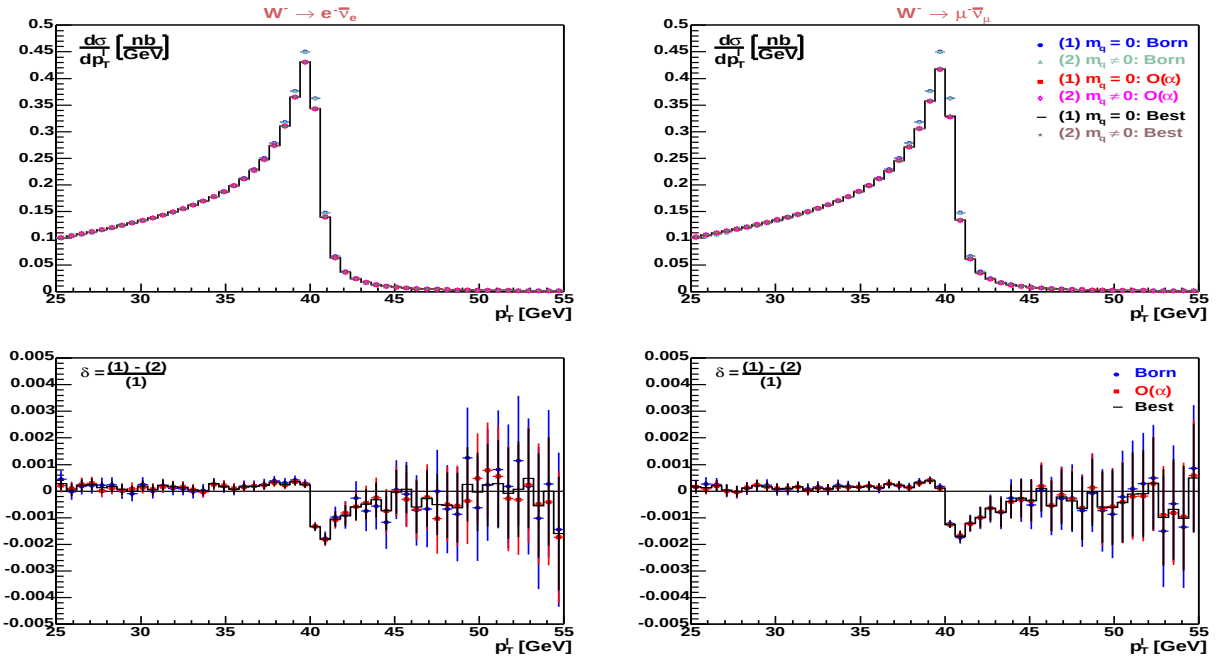

Figure 38: The quark-mass effects in the "light-cone-like scheme" for the charged lepton transverse momentum distribution of W^- production at the Born, $\mathcal{O}(\alpha)$ and "Best" levels, obtained from WINHAC. The results are shown for the electron (left) and muon (right) channels.

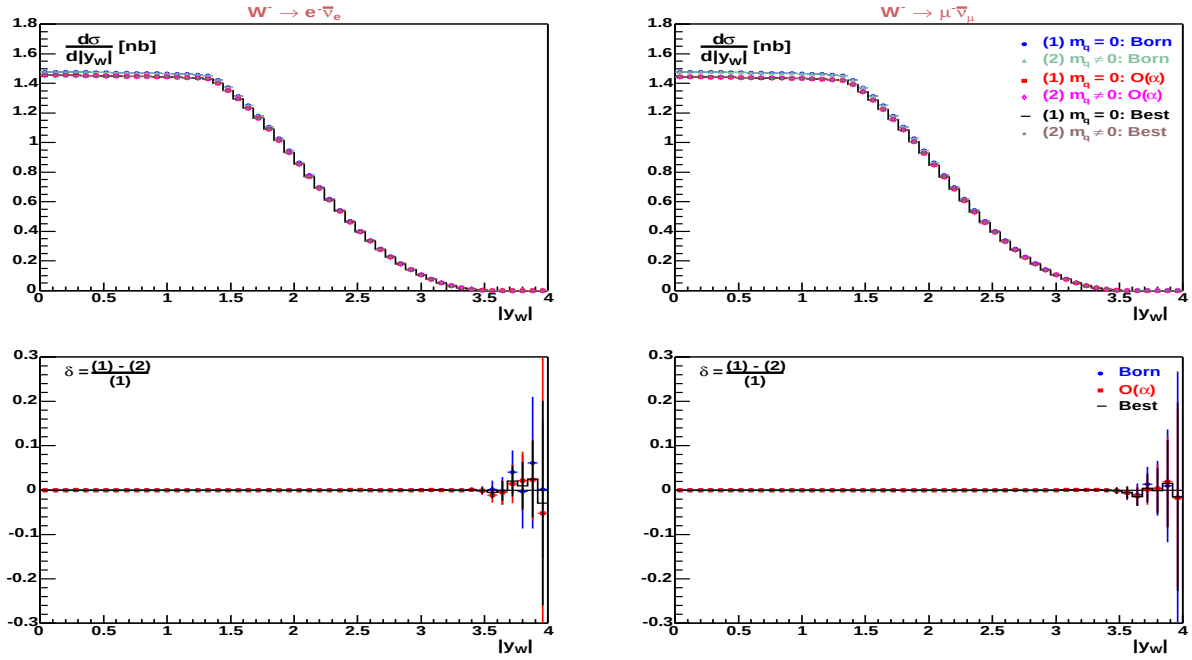

Figure 39: The quark-mass effects in the "light-cone-like scheme" for the W^- rapidity distribution at the Born, $\mathcal{O}(\alpha)$ and "Best" levels, obtained from WINHAC. The results are shown for the electron (left) and muon (right) channels.

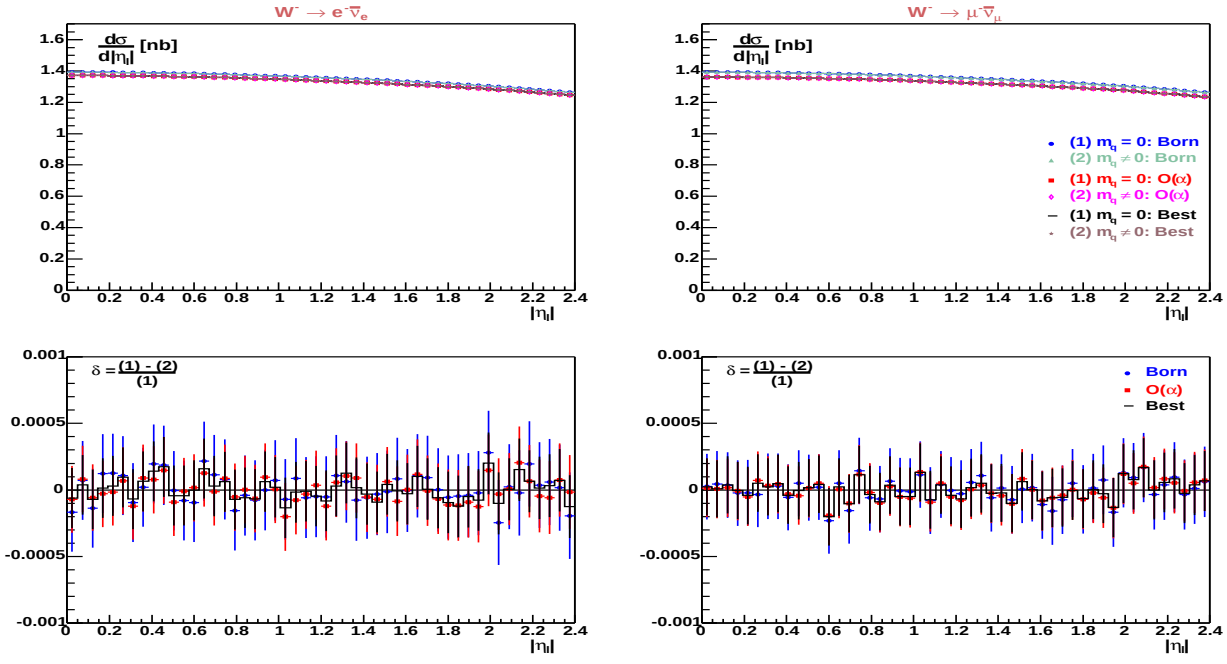

Figure 40: The quark-mass effects in the "light-cone-like scheme" for the charged lepton pseudorapidity distribution of W^- production at the Born, $\mathcal{O}(\alpha)$ and "Best" levels, obtained from WINHAC. The results are shown for the electron (left) and muon (right) channels.